

Two-photon atomic level widths at finite temperaturesT. Zaliialutdinov , A. Anikin, and D. Solovyev *Department of Physics, Saint Petersburg State University, Petrodvorets, Oulianovskaya 1, 198504 St. Petersburg, Russia*

(Received 6 June 2020; accepted 10 August 2020; published 2 September 2020)

The thermal two-photon level broadening of the excited energy levels in the hydrogen and H-like helium is evaluated via the imaginary part of thermal two-loop self-energy correction for bound electrons. All the derivations are presented in the framework of rigorous quantum electrodynamic theory at finite temperatures and are applicable for the H-like ions. On this basis, we found a contribution to the level broadening induced by the blackbody radiation which is fundamentally different from the usual line broadening caused by the stimulated two-photon decay and the Raman scattering of thermal photons. Numerical calculations of the two-loop thermal correction to the two-photon width for the $2s$ state in hydrogen and singly ionized helium atoms show that the effect could significantly exceed the higher-order relativistic and radiative QED corrections commonly included in the calculations. In addition, the thermal two-loop self-energy correction significantly exceeds the “ordinary” stimulated one-photon depopulation rate at the relevant laboratory temperatures. In this work, detailed analysis and the corresponding comparison of the effect with the existing laboratory measurements in H-like ions are carried out.

DOI: [10.1103/PhysRevA.102.032204](https://doi.org/10.1103/PhysRevA.102.032204)**I. INTRODUCTION**

During the last decades two-photon processes became of high interest in fundamental investigations of field theories, astrophysics, laboratory experiments, constructing of atomic clocks, chemistry, and biology [1–8]. Since the early days of quantum mechanics, a special role was assigned to the two-photon decay of the $2s$ state in the hydrogen atom [9]. Recent accurate measurements of the temperature and the polarization distribution of the cosmic microwave background (CMB) renewed interest in this process [8,10]. The modern theory of the cosmological recombination starts from works by Zel’dovich, Kurt, and Sunyaev [11] and Peebles [12]. In particular, the $2s \rightarrow 1s + 2\gamma(E1)$ decay rate in hydrogen was found to be the main channel within the bound-bound transitions for the radiation escape from the matter and formation of CMB. Hence the present properties of the CMB are strongly dependent on the particular qualities of the two-photon processes during the cosmological recombination epoch. In addition to the transition $2s \rightarrow 1s + 2\gamma(E1)$, no less attention is paid to the two-photon decays of excited states with principal quantum number $n > 2$, whose total contribution to the ionization fraction of primordial plasma reaches the percent level and exceeds the accuracy of CMB measurements [8,13,14].

However, the study of two-photon transitions for excited states is complicated by the crucial difference between the decays of nl ($n > 2$) and $2s$ atomic levels. This difference is determined by the presence of cascade transitions as the dominant decay channels of the excited levels which are absent in the case of $2s$ level. In connection with the presence of a cascade channel (resonant transitions), the problem of the separating of nonresonant two-photon emission

(resulting in the immediate radiation escape from the matter) arose in astrophysical studies. This question was studied within the quantum mechanical approach in a number of works (see, for example, Refs. [8,13]). Within the framework of QED theory the ambiguity of such separation was demonstrated in Refs. [15–17], while an alternative approach to obtaining a “pure” two-photon contribution based on an evaluation of the imaginary part of the two-loop self-energy of bound electrons was proposed in Refs. [18–21]. According to this “alternative” approach the found contributions were called “two-photon widths” since in the absence of cascade emission (the case of the $2s$ state in a hydrogen atom) it coincides with the two-photon transition rate [18–21]. However, within the framework of the line profile approach [22] it was shown that the imaginary part of the two-loop radiative level shift does not coincide with the two-photon decay rate for higher states and should be considered only as a radiative correction to the level widths [23] (see also Ref. [24]). The study of radiative correction of this type (but in the thermal case) according to the “alternative” method suggested in Refs. [18–21] is the main purpose of present work and we use the designation “two-loop width” assuming the imaginary part of a two-loop self-energy radiative correction to the energy level.

Besides the spontaneous decays, the corresponding transitions induced by the blackbody radiation (BBR) are also of particular interest. Accounting for the induced level broadening leads to an additional correction to CMB properties. A comprehensive analysis of the induced two-photon transitions in recombination processes based on the quantum mechanical approach has been the subject of discussion in Refs. [25–27]. However, the necessity to use the quantum

electrodynamics (QED) theory was recently demonstrated in Refs. [28–31] (see also Refs. [32,33]). Since the CMB has an almost Planck spectrum, the atomic line broadening can be described within the framework of QED for bound states at finite temperatures [34].

Particular attention can be paid to the analysis of CMB properties and the corresponding determination of the $2s$ state lifetime in a hydrogen atom with an 8% error, which is much better than in any existing laboratory experiments [35]. Nonetheless, despite a special astrophysical role of the $2s$ state in the hydrogen atom, its importance is even more significant for the laboratory spectroscopic experiments. Being especially metastable, this state allows precision measurements of various transition frequencies with an accuracy reaching 10^{-13} of relative magnitude in hydrogen, which are pursued to improve optical standards of frequency, accurate determination of physical constants, and testing of fundamental interactions in hydrogen and H-like atomic systems. To accomplish this intention, an accurate theoretical calculation of the two-photon widths of metastable states is also of experimental importance. The results of laboratory measurements of the $2s$ state lifetime in a hydrogen atom can be found in Refs. [36–38], and the results for the singly ionized helium can be found in Ref. [39]. The experimental data for the H-like highly charged ions (HCI) can be found, for example, in Refs. [40–46]. Generally speaking, experiments on measuring the natural widths of energy levels are incredibly complicated. Improving the accuracy of an experiment requires controlling the impact of physical conditions, such as the influence of external fields, Doppler broadening, evaluation of QED corrections, and such tiny effects as the Stark shifts and level broadening induced by BBR [47,48].

The formalism of thermal QED theory for bound states developed in Refs. [34] allows one to take into account more complex effects revealing the impact of thermal environment on atomic systems [32,33]. Following this theory, we investigate the two-photon level broadening caused by the “heat bath” employing the “alternative approach” [18–21] to evaluate the imaginary part of the two-loop self-energy corrections for a bound electron. The “heat bath” acting on the atomic system implies an environment described by blackbody radiation, i.e., the photon field distributed according to Planck’s law.

The paper is organized as follows. In Sec. II the general equations for the induced two-photon transitions and Raman scattering of thermal photons are given. The derivation of two-photon decay widths at finite temperatures within the two-loop approach is given in Sec. III and the corresponding expressions are presented in Sec. IV within the non-relativistic limit. All the derivations are presented in the framework of rigorous quantum electrodynamics theory at finite temperatures and are applicable for the H-like ions. The results of numerical calculations of the thermal two-photon decay widths for hydrogen and singly ionized helium atoms and their comparison with the existing laboratory measurements are discussed in Sec. V. Throughout the paper we use the relativistic units $\hbar = m_e = c = 1$ (m_e is the electron rest mass, c is the speed of light, and \hbar is the reduced Planck constant).

II. INDUCED TWO-PHOTON TRANSITIONS AND RAMAN SCATTERING IN HYDROGEN

In this section, a description of the two-photon transition rates in hydrogen in the presence of blackbody radiation (BBR) is given briefly. In the absence of external fields, only spontaneous decays of atomic states are possible. Isotropic external radiation, such as BBR, leads to additional level broadening due to the processes of thermal radiation, absorption, and Raman scattering. In the nonrelativistic limit and the electric dipole approximation, the total rate of the two-photon decay $a \rightarrow b + 2\gamma(E1)$ [$a(b)$ denotes the standard set of quantum numbers $n_{a(b)}l_{a(b)}$, where $n_{a(b)}$ is the principal quantum number of the state $a(b)$ and $l_{a(b)}$ is the corresponding orbital angular momentum] in hydrogenlike atoms after the integration over photon directions, summation over photon polarizations, averaging over the projections m_a of the initial state, and summation over projection of the final state m_b (see Ref. [24]) transforms to

$$W_{ab}^{2\gamma,\text{tot}} = \frac{1}{2} \int_0^{\omega_0} dW_{ab}^{2\gamma,\text{tot}}. \quad (1)$$

Here $dW_{ab}^{2\gamma,\text{tot}} = dW_{ab}^{2\gamma,\text{spon}} + dW_{ab}^{2\gamma,\text{ind}}$, $\omega_0 = |E_a - E_b|$ is the transition energy, and the differential spontaneous decay rate is expressed by

$$dW_{ab}^{2\gamma,\text{spon}} = \frac{8e^4}{9\pi} \frac{\omega^3(\omega_0 - \omega)^3}{2l_a + 1} \sum_{m_a m_b} \left| \sum_n \left(\frac{\langle b|\mathbf{r}|n\rangle\langle n|\mathbf{r}|a\rangle}{E_n - E_a + \omega} + \frac{\langle b|\mathbf{r}|n\rangle\langle n|\mathbf{r}|a\rangle}{E_n - E_b - \omega} \right) \right|^2 d\omega. \quad (2)$$

The differential induced decay rate corresponding to the emission process can be obtained in the following form:

$$dW_{ab}^{2\gamma,\text{ind}} = \frac{8e^4}{9\pi} \frac{\omega^3(\omega_0 - \omega)^3}{2l_a + 1} \sum_{m_a m_b} \left| \sum_n \left(\frac{\langle b|\mathbf{r}|n\rangle\langle n|\mathbf{r}|a\rangle}{E_n - E_a + \omega} + \frac{\langle b|\mathbf{r}|n\rangle\langle n|\mathbf{r}|a\rangle}{E_n - E_b - \omega} \right) \right|^2 \times [n_\beta(\omega) + n_\beta(\omega_0 - \omega) + n_\beta(\omega)n_\beta(\omega_0 - \omega)]d\omega. \quad (3)$$

In Eq. (3), $n_\beta(\omega) = (e^{\beta\omega} - 1)^{-1}$ represents the Planck distribution function giving the mean occupation number of photons in the BBR field, $\beta = (k_B T)^{-1}$, where T is the radiation temperature and k_B is the Boltzmann constant. In the BBR field, the two-photon absorption process $a + 2\gamma(E1) \rightarrow b$ should also be taken into account. The corresponding differential rate reduces to the following expression:

$$dW_{ab}^{2\gamma,\text{abs}} = \frac{8e^4}{9\pi} \frac{\omega^3(\omega_0 - \omega)^3}{2l_a + 1} \sum_{m_a m_b} \left| \sum_n \left(\frac{\langle b|\mathbf{r}|n\rangle\langle n|\mathbf{r}|a\rangle}{E_n - E_a - \omega} + \frac{\langle b|\mathbf{r}|n\rangle\langle n|\mathbf{r}|a\rangle}{E_n - E_b + \omega} \right) \right|^2 n_\beta(\omega)n_\beta(\omega_0 - \omega)d\omega. \quad (4)$$

In the case when $n_a = n_b \pm 1$, there are no cascade transitions (the energy denominators in these expressions are not equal to zero), the frequency distributions given by Eqs. (2)–(4) are regular, and the integral Eq. (1) is convergent. The

TABLE I. The BBR-induced $W_{2s1s}^{2\gamma,\text{ind}}$ and total two-photon transition rates $W_{2s1s}^{2\gamma,\text{tot}}$ (in s^{-1}) at different temperatures T (in Kelvin) in H and He^+ atoms. The nonrelativistic values of the spontaneous $2s \rightarrow 1s + 2\gamma(E1)$ transition rate in vacuum are $W_{2s1s}^{2\gamma,\text{spon}} = 8.229\,352\,\text{s}^{-1}$ and $5.266\,785 \times 10^2\,\text{s}^{-1}$ [49] for H and He^+ , respectively.

Atom	T	77	300	1000	3000	5000	10^4
H	$W_{2s1s}^{2\gamma,\text{ind}}$	1.358×10^{-4}	2.028×10^{-3}	2.151×10^{-2}	1.731×10^{-1}	4.389×10^{-1}	1.467
	$W_{2s1s}^{2\gamma,\text{tot}}$	8.229	8.231	8.251	8.402	8.668	9.697
He^+	$W_{2s1s}^{2\gamma,\text{ind}}$	5.438×10^{-4}	8.243×10^{-3}	9.044×10^{-2}	7.868×10^{-1}	2.118×10^{-1}	7.893
	$W_{2s1s}^{2\gamma,\text{tot}}$	5.267×10^2	5.267×10^2	5.268×10^2	5.275×10^2	5.288×10^2	5.346×10^2

results of the $dW_{ab}^{2\gamma,\text{ind}}$ evaluation, Eq. (3), for the $2s \rightarrow 1s + 2\gamma(E1)$ transition at different temperatures in a hydrogen atom (H) and singly ionized helium (He^+) are given in Table I, where the total contribution (spontaneous plus induced) is given also.

The frequency distributions for this transition in H are shown in Fig. 1, where the contribution of the induced transition depending on temperature is observed visually. Calculations show that the contribution, arising from the cross product $n_\beta(\omega)n_\beta(\omega_0 - \omega)$ in Eq. (3) and interpreted as interference of two thermal photons, is negligible up to the temperatures of the order of $T = 10^4$ K.

In addition to the usual induced emission and absorption transitions, the BBR-stimulated Stokes and anti-Stokes Raman scattering process $a + \gamma(E1) \rightarrow b + \gamma'(E1)$ should be also considered. Its differential rate can be obtained within the same methodology [50]. The result is

$$dW_{ab}^{2\gamma,\text{ram}} = \frac{8e^4 \omega^3 (\omega_0 + \omega)^3}{9\pi} \sum_{m_a m_b} \left| \sum_n \left(\frac{\langle b|\mathbf{r}|n\rangle \langle n|\mathbf{r}|a\rangle}{E_n - E_a - \omega} + \frac{\langle b|\mathbf{r}|n\rangle \langle n|\mathbf{r}|a\rangle}{E_n - E_b + \omega} \right) \right|^2 \times [n_\beta(\omega) + n_\beta(\omega)n_\beta(\omega_0 + \omega)] d\omega, \quad (5)$$

where for the Stokes process $\omega_0 = E_a - E_b < 0$ and for the anti-Stokes process $\omega_0 = E_a - E_b > 0$. The corresponding total rate is defined by $W_{ab}^{2\gamma,\text{AS-ram}} = \int_0^\infty dW_{ab}^{2\gamma,\text{ram}}$ and

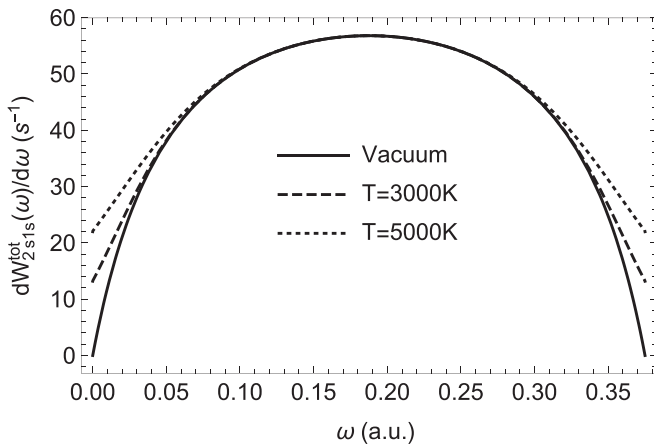


FIG. 1. Differential transition rate $dW_{2s1s}^{\text{tot}}(\omega)$ in s^{-1} for the $2s \rightarrow 1s + 2\gamma(E1)$ transition in H atoms in the presence of the BBR field with temperature T (in Kelvin). The bold line corresponds to the transition rate in the absence of the BBR field (vacuum).

$W_{ab}^{2\gamma,\text{S-ram}} = \int_{|\omega_0|}^\infty dW_{ab}^{2\gamma,\text{ram}}$ for anti-Stokes and Stokes processes, respectively.

For the hydrogen atom with the fixed $a = 2s$ and $b = 1s$ states the corresponding distribution of the anti-Stokes scattering rate is shown in Fig. 2. In particular, from Fig. 2 it follows that the induced cascade contributions in the Raman scattering become significant with the increasing of temperature.

III. TWO-LOOP ELECTRON SELF-ENERGY WITH ONE AND TWO THERMAL LOOPS

Until now, the well-known effects arising in the BBR field were considered. The results expressed by Eqs. (2)–(5) can be easily obtained within the framework of the quantum mechanical approach. The same can be found within the rigorous QED theory in approximation of zero level widths of bound states. Nevertheless, the application of QED theory can be used to identify new effects (see, for example, Ref. [28]). In particular, within the framework of the QED perturbation theory for a bound electron, such self-energy radiative corrections as the one-loop (second-order in the coupling constant), two-loop (fourth-order in the coupling constant), etc., can be treated as sequential contributions. In the absence of external fields and cascades, the imaginary parts of these corrections give the one-photon width $\Gamma_a^{1\gamma}$, the two-photon width $\Gamma_a^{2\gamma}$, etc.. Then the total level width Γ_a of the atomic state a can be

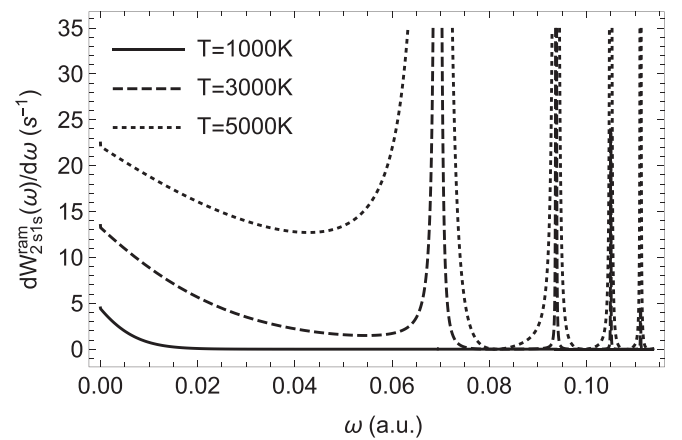


FIG. 2. Differential transition rate $dW_{2s1s}^{\text{ram}}(\omega)$ in s^{-1} for the Raman scattering of BBR photons on H atoms in the process $2s \rightarrow 1s + \gamma(E1)$. The BBR field temperature is denoted as T (in Kelvin). Sharp peaks correspond to resonances in Eq. (5).

TABLE II. BBR-induced level widths $\Gamma_{2s}^{1\gamma, \text{BBR}}$ [see Eq. (11)] and $\Gamma_{2s}^{1\gamma, \text{BBR-QED}}$ [see Eq. (12)] in s^{-1} at different temperatures T (in Kelvin) for H and He^+ atoms. The Lamb shift $2p-2s$ is taken into account [52]. The values marked with * and ** are taken from Refs. [28,47] and [53], respectively.

Atom	T	77	300	1000	3000	5000	10^4
H	$\Gamma_{2s}^{1\gamma, \text{BBR}}$	3.653×10^{-6}	1.423×10^{-5} 1.42×10^{-5} *	2.023×10^{-2}	4.701×10^4 4.706×10^4 **	9.671×10^5	1.248×10^7
	$\Gamma_{2s}^{1\gamma, \text{BBR-QED}}$	2.766×10^{-4}	4.159×10^{-3}	6.633×10^{-2}	4.701×10^4	9.671×10^5	1.248×10^7
	$\Gamma_{3s}^{1\gamma, \text{BBR}}$	2.328×10^{-6}	8.035×10^{-5} 7.97×10^{-5} *	4.346×10^3	9.903×10^5	4.042×10^6	1.772×10^7
He^+	$\Gamma_{3s}^{1\gamma, \text{BBR-QED}}$	5.148×10^{-4}	7.865×10^{-3}	4.346×10^3	9.903×10^5	4.042×10^6	1.772×10^7
	$\Gamma_{2s}^{1\gamma, \text{BBR}}$	1.599×10^{-4}	6.249×10^{-4}	2.085×10^{-3}	6.472×10^{-3}	25.97	1.712×10^5
	$\Gamma_{2s}^{1\gamma, \text{BBR-QED}}$	1.251×10^{-3}	1.720×10^{-2}	1.863×10^{-1}	1.665	30.58	1.712×10^5
	$\Gamma_{3s}^{1\gamma, \text{BBR}}$	8.596×10^{-5}	3.352×10^{-4}	1.125×10^{-3}	5.318×10^3	3.296×10^5	8.621×10^6
	$\Gamma_{3s}^{1\gamma, \text{BBR-QED}}$	4.053×10^{-3}	6.057×10^{-2}	6.708×10^{-1}	5.324×10^3	3.296×10^5	8.621×10^6

presented by the infinite series

$$\Gamma_a = \Gamma_a^{1\gamma} + \Gamma_a^{2\gamma} + \dots \quad (6)$$

In turn, the natural one-photon width $\Gamma_a^{1\gamma}$ is equal to the sum of the one-photon transition rates to lower levels. In the nonrelativistic limit it can be written as follows:

$$\Gamma_a^{1\gamma} = \frac{4e^2}{3} \frac{1}{2l_a + 1} \sum_{b < a} \sum_{m_a m_b} \omega_{ab}^3 | \langle b | \mathbf{r} | a \rangle |^2, \quad (7)$$

where $\omega_{ab} = E_a - E_b$. Recently, the two-photon width $\Gamma_a^{2\gamma}$ was evaluated within the relativistic adiabatic QED theory [23], where the expression for $\Gamma_a^{2\gamma}$ was also obtained in the nonrelativistic limit:

$$\begin{aligned} \Gamma_a^{2\gamma} &= \frac{4e^4}{9\pi} \frac{1}{2l_a + 1} \lim_{\eta \rightarrow 0} \text{Re} \sum_{b < a} \sum_{m_a m_b} \int_0^{\omega_{ab}} d\omega \omega^3 (\omega_{ab} - \omega)^3 \\ &\times \sum_{m n'} \left(\frac{\langle b | \mathbf{r} | n \rangle \langle n | \mathbf{r} | a \rangle}{E_n - E_a + \omega + i\eta} + \frac{\langle b | \mathbf{r} | n \rangle \langle n | \mathbf{r} | a \rangle}{E_n - E_b - \omega + i\eta} \right) \\ &\times \left(\frac{\langle b | \mathbf{r} | n' \rangle^* \langle n' | \mathbf{r} | a \rangle^*}{E_{n'} - E_a + \omega + i\eta} + \frac{\langle b | \mathbf{r} | n' \rangle^* \langle n' | \mathbf{r} | a \rangle^*}{E_{n'} - E_b - \omega + i\eta} \right). \quad (8) \end{aligned}$$

This result was obtained at first in Ref. [18]. It is worth noting that the expression (8) coincides with Eq. (2) for the two-photon decay rate only in the absence of resonant energy denominators. Then the imaginary infinitesimal part $i\eta$ (η is the adiabatic parameter) in Eq. (8) can be omitted and the product of two terms in parentheses is equal to the square modulus, making $\Gamma_a^{2\gamma}$ the same with the spontaneous decay rate $W_a^{2\gamma, \text{spon}}$.

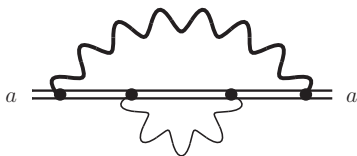


FIG. 3. Ordinary loop inside thermal loop Feynman diagram. The bold wavy line denotes the thermal photon propagator. A double line is the electron propagator in the Furry picture.

The situation is different for the two-photon transitions with cascades, i.e., when the presence of resonant intermediate states in the sum over n in Eq. (8) leads to the divergent contributions. In this case, the transition rate, Eq. (2), should be regularized in the vicinity of resonances. The regularization procedure of multiphoton transition amplitudes within the framework of QED theory can be found, for example, in Ref. [51]. As a result the corresponding level widths arise in the divergent contributions that lead to the regular expression.

In contrast, there is no need to regularize Eq. (8) (see Refs. [18–20]). In particular, in Ref. [18] it was demonstrated that the integral

$$\lim_{\eta \rightarrow 0} \text{Re} \int_0^1 d\omega \left(\frac{1}{a - \omega + i\eta} \right)^2 = \frac{1}{a(a-1)} + O(\eta^2) \quad (9)$$

is finite, when the limit is taken after integration over the frequency ω (here it is assumed that $0 < a < 1$). With that, the integral, arising in the expression for the two-photon transition rate or Raman scattering rate, is divergent when $\eta \rightarrow 0$:

$$\int_0^1 d\omega \left| \frac{1}{a - \omega + i\eta} \right|^2 = \frac{\pi}{\eta} + \frac{1}{a(a-1)} + O(\eta^2). \quad (10)$$

The integration method corresponding to Eq. (9) was also justified in Ref. [23] within the adiabatic S -matrix formalism. However, in opposite to Ref. [18] the main conclusion is that the contribution Eq. (8) represents the radiative correction to the one-photon level widths, but not the two-photon transition rate since it can be negative (see Refs. [23,24]).

In the presence of BBR, there is an additional line broadening due to the induced transitions. Within the framework of finite temperature QED for bound states [34], the induced

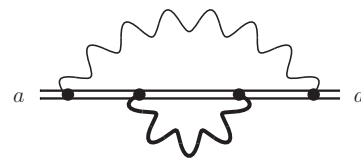


FIG. 4. Thermal loop inside ordinary loop Feynman diagram. All the notations are the same as those in Fig. 3.

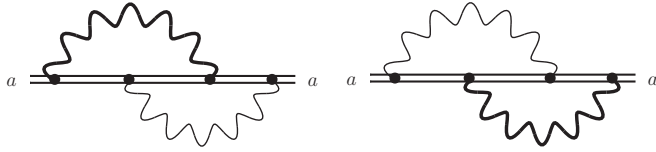


FIG. 5. Thermal loop over ordinary loop.

one-photon width $\Gamma_a^{1\gamma, \text{BBR}}$ is given by the imaginary part of thermal one-loop electron self-energy [28]. In the nonrelativistic limit, the result of such evaluation leads to the well-known quantum mechanical expression [47], which is

$$\Gamma_a^{1\gamma, \text{BBR}} = \frac{4e^2}{3} \frac{1}{2l_a + 1} \sum_b \sum_{m_a m_b} |\omega_{ab}|^3 |\langle b | \mathbf{r} | a \rangle|^2 n_\beta(|\omega_{ab}|). \quad (11)$$

Here, summation over states b extends to the entire spectrum of the Schrödinger equation, including upper, lower, and continuum states.

In Ref. [28] it was shown that the expression (11) arises in the framework of the QED theory in the approximation of zero level widths. In turn, taking into account the finite lifetimes of atomic levels, the more general expression for the one-photon BBR-induced line broadening can be obtained as

$$\Gamma_a^{1\gamma, \text{BBR-QED}} = \frac{2e^2}{3\pi} \frac{1}{2l_a + 1} \sum_b \sum_{m_a m_b} |\langle a | \mathbf{r} | b \rangle|^2 \int_0^\infty d\omega n_\beta(\omega) \omega^3 \times \left[\frac{\Gamma_{ba}}{(\tilde{\omega}_{ba} + \omega)^2 + \frac{1}{4}\Gamma_{ba}^2} + \frac{\Gamma_{ba}}{(\tilde{\omega}_{ba} - \omega)^2 + \frac{1}{4}\Gamma_{ba}^2} \right], \quad (12)$$

where $\Gamma_{ba} = \Gamma_b + \Gamma_a$ is the sum of natural widths of states b and a . It is easy to see that, in the limit $\Gamma_{ba} \rightarrow 0$, Eq. (12) turns to Eq. (11). The comparison of $\Gamma_{2s}^{1\gamma, \text{BBR}}$ and $\Gamma_{2s}^{1\gamma, \text{BBR-QED}}$ for the $2s$ state in H and He^+ atoms is presented in Table II. In particular, it can be found that the accounting for finite lifetimes plays an important role in the broadening of the $2s$ state at low temperatures and is negligible at high temperatures (see also Ref. [31]).

Finally, the total level widths of the atomic state a in the presence of the BBR field can be written as

$$\Gamma_a^{\text{tot}} = \Gamma_a + \Gamma_a^{\text{BBR}}, \quad (13)$$

where Γ_a is the “zero-temperature” contribution, Eq. (6), and

$$\Gamma_a^{\text{BBR}} = \Gamma_a^{1\gamma, \text{BBR}} + \Gamma_a^{2\gamma, \text{BBR}} + \dots \quad (14)$$

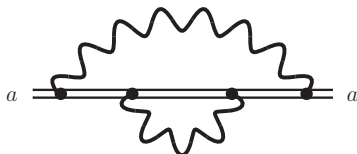


FIG. 6. Thermal loop inside thermal loop.

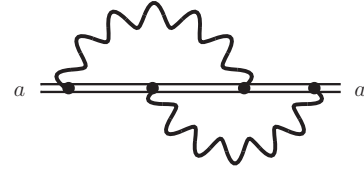


FIG. 7. Thermal loop over thermal loop.

represents the contributions (one-photon, two-photon, etc., respectively) corresponding to the BBR-induced level broadening.

To describe the thermal-induced two-photon contribution to the level broadening, $\Gamma_a^{2\gamma, \text{BBR}}$, that arises in an atom under the influence of blackbody radiation, we employ the formalism of QED theory at finite temperatures (see, for example, Ref. [34] and references therein). To take into account the “heat bath” influence on an atom in the framework of this formalism, it is sufficient to consider sequentially the insertions of the thermal part of the photon propagator instead of the ordinary one in the Feynman graphs, which are Figs. 3–7 in our case. As a result, the imaginary part of two-loop SE corrections (Figs. 3–7), in addition to the two-photon processes, contains also the thermal radiative corrections to the one-photon transitions [54]. Recently, these contributions were considered in Ref. [33] and we omit their description here. In turn, the induced two-photon decay widths result from the integration over the pole in the middle electron propagator of the irreducible Feynman diagrams depicted in Figs. 3–7 [54,55].

According to Ref. [56], the corrections ΔE_a to the energy of the state a for any irreducible graphs can be obtained using the relations

$$\Delta E_a = \langle a | \hat{U}_{\text{irr}} | a \rangle, \quad (15)$$

where $\langle a' | \hat{U}_{\text{irr}} | a \rangle$ is the matrix element of amplitude of the S matrix:

$$\langle a' | \hat{S} | a \rangle = -2\pi i \delta(E_{a'} - E_a) \langle a' | \hat{U}_{\text{irr}} | a \rangle. \quad (16)$$

Then the two-photon radiative correction to the level width is defined by the imaginary part of the second-order SE level shift $\Delta E_a^{(2)}$, which is given by the sum of Feynman diagrams shown in Figs. 3–7. The result can be presented as

$$\Gamma_a^{2\gamma} = -2\text{Im} \Delta E_a^{(2)}. \quad (17)$$

It should be noted here again that the expression (17) reproduces the two-photon level width in the absence of cascade processes and is merely the radiative correction in the general case. Further, we give the step-by-step description of each diagram in Figs. 3–7 within the S -matrix formalism. For clarity, the replacements of the “ordinary” loop by the thermal one (one and two times) are denoted by the bold wavy line in the each irreducible graph.

A. Ordinary loop inside thermal loop

We start from the consideration of Fig. 3. The corresponding S -matrix element is

$$\hat{S}_{aa}^{(4)\text{Fig.3}} = (-ie)^4 \int d^4x_1 d^4x_2 d^4x_3 d^4x_4 \bar{\psi}_a(x_4) \gamma_{\mu_4} S(x_4x_3) \gamma_{\mu_3} S(x_3x_2) \gamma_{\mu_2} S(x_2x_1) \gamma_{\mu_1} \psi_a(x_1) D_{\mu_4\mu_1}^\beta(x_4x_1) D_{\mu_3\mu_2}(x_3x_2). \quad (18)$$

Here $\psi_a(x) = \psi_a(\mathbf{r})e^{-iE_a t}$, $\psi_a(\mathbf{r})$ is the solution of the Dirac equation for the atomic electron, E_a is the Dirac energy, $\bar{\psi}_a = \psi_a^\dagger \gamma_0$ is the Dirac conjugated wave function with ψ_a^\dagger being its Hermitian conjugate, $\gamma_\mu = (\gamma_0, \boldsymbol{\gamma})$ are the Dirac matrices, $S(x_1, x_2)$ is the electron propagator, $D_{\mu_i\mu_j}(x_i x_j)$ is the ‘‘ordinary’’ photon propagator, and $D_{\mu_i\mu_j}^\beta(x_i x_j)$ is the thermal photon propagator. The eigenmode decomposition of $S(x_1, x_2)$ with respect to one-electron eigenstates is

$$S(x_1, x_2) = \frac{i}{2\pi} \int_{-\infty}^{\infty} d\Omega e^{-i\Omega(t_1-t_2)} \sum_n \frac{\psi_n(\mathbf{r}_1) \bar{\psi}_n(\mathbf{r}_2)}{\Omega - E_n(1-i0)}, \quad (19)$$

where summation runs over the entire Dirac spectrum. The ‘zero-temperature’ photon propagator in the Feynman gauge is

$$D_{\mu_i\mu_j}(x_i x_j) = \frac{1}{2\pi i} \frac{g_{\mu_i\mu_j}}{r_{ij}} \int_{-\infty}^{\infty} d\omega e^{i\omega(t_i-t_j)+i|\omega|r_{ij}}, \quad (20)$$

while the thermal part $D_{\mu_i\mu_j}^\beta(x_i x_j)$ can be reduced to [28,34]

$$D_{\mu_i\mu_j}^\beta(x_i x_j) = -\frac{g_{\mu_i\mu_j}}{\pi r_{12}} \int_{-\infty}^{\infty} d\omega n_\beta(|\omega|) \sin(|\omega|r_{ij}) e^{-i\omega(t_i-t_j)}. \quad (21)$$

Then, performing integration over time variables in Eq. (18) and using Eq. (16), the amplitude of the process shown in Fig. 3 is given by

$$U_a^{\text{Fig.3}} = \sum_{n_1 n_2 n_3} \frac{-ie^4}{2\pi^2} \int_{-\infty}^{\infty} \int_{-\infty}^{\infty} d\omega_1 d\omega_2 n_\beta(|\omega_1|) \left[\frac{1 - \alpha_1 \alpha_4}{r_{14}} \sin(|\omega_1| r_{14}) \right]_{an_1 n_3 a} \left[\frac{1 - \alpha_2 \alpha_3}{r_{23}} e^{i|\omega_2| r_{23}} \right]_{n_2 n_3 n_1 n_2} \times \frac{1}{[E_{n_3}(1-i0) - E_a + \omega_1][E_{n_2}(1-i0) - E_a + \omega_1 + \omega_2][E_{n_1}(1-i0) - E_a + \omega_1]}. \quad (22)$$

The matrix elements $[F(12)]_{abcd}$ should be understood as $[F(12)]_{a(1)b(2)c(1)d(2)}$, where indexes 1 and 2 denote the variables and α_i are the Dirac matrices.

As it is mentioned above, the two-photon contribution to the level widths is defined by the pole contribution in the middle electron propagator of Eq. (22). The corresponding integration over ω_2 in Eq. (22) can be performed with the use of the Cauchy theorem. Repeating the procedure described in Ref. [56], one can obtain

$$\int_{-\infty}^{\infty} d\omega_2 \frac{e^{i|\omega_2| r_{23}}}{E_{n_2}(1-i0) - E_a + \omega_1 + \omega_2} = \frac{\pi i}{2} \left(1 + \frac{E_{n_2}}{|E_{n_2}|} \right) \left(1 - \frac{\omega_{n_2 a} + \omega_1}{|\omega_{n_2 a} + \omega_1|} \right) e^{i|\omega_{n_2 a} + \omega_1| r_{23}} + 2i \frac{\omega_{n_2 a} + \omega_1}{|\omega_{n_2 a} + \omega_1|} [\text{ci}(|\omega_{n_2 a} + \omega_1| r_{ij}) \sin(|\omega_{n_2 a} + \omega_1| r_{23}) - \text{si}(|\omega_{n_2 a} + \omega_1| r_{ij}) \cos(|\omega_{n_2 a} + \omega_1| r_{23})], \quad (23)$$

where $\omega_{n_2 a} = E_{n_2} - E_a$. Then substituting Eq. (22) into Eq. (17), using Eq. (23), and taking into account the explicit insertion of the remaining modulus sign, we arrive at

$$\Gamma_a^{\text{Fig.3}} = \frac{2e^4}{\pi} \sum_{n_1 n_2 n_3} \left\{ \text{Re} \int_0^\infty d\omega_1 n_\beta(\omega_1) \left[\frac{1 - \alpha_1 \alpha_4}{r_{14}} \sin(\omega_1 r_{14}) \right]_{an_2 n_3 a} \left[\frac{1 - \alpha_2 \alpha_3}{r_{23}} \sin(|\omega_{n_2 a} - \omega_1| r_{23}) \right]_{n_2 n_3 n_1 n_2} \times \frac{1}{[E_{n_3}(1-i0) - E_a - \omega_1][E_{n_1}(1-i0) - E_a - \omega_1]} \left[\frac{\pi}{2} \left(1 + \frac{E_{n_2}}{|E_{n_2}|} \right) \left(1 - \frac{\omega_{n_2 a} - \omega_1}{|\omega_{n_2 a} - \omega_1|} \right) \right] + \text{Re} \int_0^\infty d\omega_1 n_\beta(\omega_1) \left[\frac{1 - \alpha_1 \alpha_4}{r_{14}} \sin(\omega_1 r_{14}) \right]_{an_2 n_3 a} \left[\frac{1 - \alpha_2 \alpha_3}{r_{23}} \sin(|\omega_{n_2 a} + \omega_1| r_{23}) \right]_{n_2 n_3 n_1 n_2} \times \frac{1}{[E_{n_3}(1-i0) - E_a + \omega_1][E_{n_1}(1-i0) - E_a + \omega_1]} \left[\frac{\pi}{2} \left(1 + \frac{E_{n_2}}{|E_{n_2}|} \right) \left(1 - \frac{\omega_{n_2 a} + \omega_1}{|\omega_{n_2 a} + \omega_1|} \right) \right] \right\}. \quad (24)$$

For further evaluation, the two cases should be considered separately: $\omega_{n_2 a} > 0$ and $\omega_{n_2 a} < 0$. First, $\omega_{n_2 a} > 0$, and then the second integral in Eq. (24) vanishes, because $\omega_{n_2 a} + \omega_1$ is always positive, and the integration interval runs through the positive

half-axis. Then, for the positive energies $E_{n_2} > 0$, Eq. (24) reduces to

$$\Gamma_a^{\text{Fig. 3}} = \frac{2e^4}{\pi} \sum_{n_1 n_2 n_3} \text{Re} \int_{|\omega_{n_2 a}|}^{\infty} d\omega n_\beta(\omega) \left[\frac{1 - \alpha_1 \alpha_4}{r_{14}} \sin(\omega r_{14}) \right]_{a n_1 n_3 a} \left[\frac{1 - \alpha_2 \alpha_3}{r_{23}} \sin[(\omega - |\omega_{n_2 a}|) r_{23}] \right]_{n_2 n_3 n_1 n_2} \times \frac{1}{[E_{n_3}(1 - i0) - E_a - \omega][E_{n_1}(1 - i0) - E_a - \omega]}. \quad (25)$$

For the second case, $\omega_{n_2 a} < 0$, and positive energies $E_{n_2} > 0$, Eq. (24) transforms to

$$\Gamma_a^{\text{Fig. 3}} = \frac{2e^4}{\pi} \sum_{n_1 n_2 n_3} \text{Re} \int_0^{\infty} d\omega n_\beta(\omega) \left[\frac{1 - \alpha_1 \alpha_4}{r_{14}} \sin(\omega r_{14}) \right]_{a n_1 n_3 a} \left[\frac{1 - \alpha_2 \alpha_3}{r_{23}} \sin[(|\omega_{n_2 a}| + \omega) r_{23}] \right]_{n_2 n_3 n_1 n_2} \times \frac{1}{[E_{n_3}(1 - i0) - E_a - \omega][E_{n_1}(1 - i0) - E_a - \omega]} + \frac{2e^4}{\pi} \sum_{n_1 n_2 n_3} \text{Re} \int_0^{|\omega_{n_2 a}|} d\omega n_\beta(\omega) \left[\frac{1 - \alpha_1 \alpha_4}{r_{14}} \sin(\omega r_{14}) \right]_{a n_1 n_3 a} \left[\frac{1 - \alpha_2 \alpha_3}{r_{23}} \sin[(|\omega_{n_2 a}| - \omega) r_{23}] \right]_{n_2 n_3 n_1 n_2} \times \frac{1}{[E_{n_3}(1 - i0) - E_a + \omega][E_{n_1}(1 - i0) - E_a + \omega]}. \quad (26)$$

It is shown below, see Sec. IV, that Eq. (25) and the first term in Eq. (26) represent a part of the thermal correction to the level broadening associated with the Stokes and anti-Stokes Raman scattering rates of thermal photons on virtual states: $a + \gamma_T \rightarrow n_2 + \gamma$. The second term in Eq. (26) gives correction to the induced two-photon emission.

B. Thermal loop inside ordinary loop

The evaluation of the digram in Fig. 4 repeats the calculations performed in previous subsection, its S -matrix element reads

$$\hat{S}_{aa}^{(4) \text{ Fig. 4}} = (-ie)^4 \int d^4 x_1 d^4 x_2 d^4 x_3 d^4 x_4 \bar{\psi}_a(x_4) \gamma_{\mu_4} S(x_4 x_3) \gamma_{\mu_3} S(x_3 x_2) \gamma_{\mu_2} S(x_2 x_1) \gamma_{\mu_1} \psi_a(x_1) D_{\mu_4 \mu_1}(x_4 x_1) D_{\mu_3 \mu_2}^\beta(x_3 x_2). \quad (27)$$

Integration over the time variables in Eq. (27) leads to the following amplitude:

$$U_a^{\text{Fig. 4}} = \frac{-ie^4}{2\pi^2} \sum_{n_1 n_2 n_3} \int_{-\infty}^{\infty} \int_{-\infty}^{\infty} d\omega_1 d\omega_2 n_\beta(|\omega_1|) \left[\frac{1 - \alpha_1 \alpha_4}{r_{23}} \sin(|\omega_1| r_{23}) \right]_{a n_1 n_3 a} \left[\frac{1 - \alpha_2 \alpha_3}{r_{14}} e^{i|\omega_2| r_{14}} \right]_{n_2 n_3 n_1 n_2} \times \frac{1}{[E_{n_3}(1 - i0) - E_a + \omega_2][E_{n_2}(1 - i0) - E_a + \omega_1 + \omega_2][E_{n_1}(1 - i0) - E_a + \omega_2]}. \quad (28)$$

Performing integration over ω_2 in Eq. (28) with the use of Eq. (23), for $\omega_{n_2 a} > 0$, we arrive at

$$\Gamma_a^{\text{Fig. 4}} = \frac{2e^4}{\pi} \sum_{n_1 n_2 n_3} \text{Re} \int_{|\omega_{n_2 a}|}^{\infty} d\omega n_\beta(\omega) \left[\frac{1 - \alpha_2 \alpha_3}{r_{23}} \sin(\omega r_{23}) \right]_{a n_1 n_3 a} \left[\frac{1 - \alpha_1 \alpha_4}{r_{14}} \sin[(\omega - |\omega_{n_2 a}|) r_{14}] \right]_{n_2 n_3 n_1 n_2} \times \frac{1}{[E_{n_3}(1 - i0) - E_{n_2} + \omega][E_{n_1}(1 - i0) - E_{n_2} + \omega]}, \quad (29)$$

and for $\omega_{n_2 a} < 0$, we have

$$\Gamma_a^{\text{Fig. 4}} = \frac{2e^4}{\pi} \sum_{n_1 n_2 n_3} \text{Re} \int_0^{\infty} d\omega n_\beta(\omega) \left[\frac{1 - \alpha_2 \alpha_3}{r_{23}} \sin(\omega r_{23}) \right]_{a n_1 n_3 a} \left[\frac{1 - \alpha_1 \alpha_4}{r_{14}} \sin[(|\omega_{n_2 a}| + \omega) r_{14}] \right]_{n_2 n_3 n_1 n_2} \times \frac{1}{[E_{n_3}(1 - i0) - E_{n_2} + \omega][E_{n_1}(1 - i0) - E_{n_2} + \omega]} + \frac{2e^4}{\pi} \sum_{n_1 n_2 n_3} \text{Re} \int_0^{|\omega_{n_2 a}|} d\omega n_\beta(\omega) \left[\frac{1 - \alpha_2 \alpha_3}{r_{23}} \sin(\omega r_{23}) \right]_{a n_1 n_3 a} \left[\frac{1 - \alpha_1 \alpha_4}{r_{14}} \sin[(|\omega_{n_2 a}| - \omega) r_{14}] \right]_{n_2 n_3 n_1 n_2} \times \frac{1}{[E_{n_3}(1 - i0) - E_{n_2} - \omega][E_{n_1}(1 - i0) - E_{n_2} - \omega]}. \quad (30)$$

C. Thermal loop over ordinary loop

The contribution corresponding to the Feynman graph depicted in Fig. 5 is given by the following S -matrix element:

$$\hat{S}_{aa}^{(4)\text{Fig.5}} = (-ie)^4 \int d^4x_1 d^4x_2 d^4x_3 d^4x_4 \bar{\psi}_a(x_4) \gamma_{\mu_4} S(x_4x_3) \gamma_{\mu_3} S(x_3x_2) \gamma_{\mu_2} S(x_2x_1) \gamma_{\mu_1} \psi_a(x_1) D_{\mu_4\mu_2}(x_4x_2) D_{\mu_3\mu_1}^\beta(x_3x_1). \quad (31)$$

Integration over the time variables in Eq. (31) leads to the following expression for the amplitude:

$$U_a^{\text{Fig.5}} = \frac{-ie^4}{2\pi^2} \sum_{n_1 n_2 n_3} \int_{-\infty}^{\infty} \int_{-\infty}^{\infty} d\omega_1 d\omega_2 n_\beta(|\omega_1|) \left[\frac{1 - \alpha_3 \alpha_1}{r_{31}} \sin(|\omega_1| r_{31}) \right]_{an_2 n_3 n_1} \left[\frac{1 - \alpha_4 \alpha_2}{r_{42}} e^{i|\omega_2| r_{42}} \right]_{n_3 n_1 n_2 a} \\ \times \frac{1}{[E_{n_3}(1-i0) - E_a + \omega_1][E_{n_2}(1-i0) - E_a + \omega_1 + \omega_2][E_{n_1}(1-i0) - E_a + \omega_2]}. \quad (32)$$

Performing integration over ω_2 in Eq. (32), using Eq. (23), and repeating the steps described above, we obtain

$$\Gamma_a^{\text{Fig.5}} = \frac{2e^4}{\pi} \sum_{n_1 n_2 n_3} \text{Re} \int_{|\omega_{n_2 a}|}^{\infty} d\omega n_\beta(\omega) \left[\frac{1 - \alpha_3 \alpha_1}{r_{31}} \sin(\omega r_{31}) \right]_{an_2 n_3 n_1} \left[\frac{1 - \alpha_4 \alpha_2}{r_{42}} \sin[(\omega - |\omega_{n_2 a}|) r_{42}] \right]_{n_3 n_1 n_2 a} \\ \times \frac{1}{[E_{n_3}(1-i0) - E_a - \omega][E_{n_1}(1-i0) - E_{n_2} + \omega]}, \quad (33)$$

where $\omega_{n_2 a} > 0$, and for $\omega_{n_2 a} < 0$, we have

$$\Gamma_a^{\text{Fig.5}} = \frac{2e^4}{\pi} \sum_{n_1 n_2 n_3} \text{Re} \int_0^{\infty} d\omega n_\beta(\omega) \left[\frac{1 - \alpha_3 \alpha_1}{r_{31}} \sin(\omega r_{31}) \right]_{an_2 n_3 n_1} \left[\frac{1 - \alpha_4 \alpha_2}{r_{42}} \sin[(|\omega_{n_2 a}| + \omega) r_{42}] \right]_{n_3 n_1 n_2 a} \\ \times \frac{1}{[E_{n_3}(1-i0) - E_a - \omega][E_{n_1}(1-i0) - E_{n_2} + \omega]} \\ + \frac{2e^4}{\pi} \sum_{n_1 n_2 n_3} \text{Re} \int_0^{|\omega_{n_2 a}|} d\omega n_\beta(\omega) \left[\frac{1 - \alpha_3 \alpha_1}{r_{31}} \sin(\omega r_{31}) \right]_{an_2 n_3 n_1} \left[\frac{1 - \alpha_4 \alpha_2}{r_{42}} \sin[(|\omega_{n_2 a}| + \omega) r_{42}] \right]_{n_3 n_1 n_2 a} \\ \times \frac{1}{[E_{n_3}(1-i0) - E_a + \omega][E_{n_1}(1-i0) - E_{n_2} - \omega]}. \quad (34)$$

D. Thermal loop inside thermal loop

The contribution of the Feynman graph depicted in Fig. 5 corresponds to the S -matrix element:

$$\hat{S}_{aa}^{(4)\text{Fig.6}} = (-ie)^4 \int d^4x_1 d^4x_2 d^4x_3 d^4x_4 \bar{\psi}_a(x_1) \gamma_{\mu_4} S(x_1x_2) \gamma_{\mu_3} S(x_2x_3) \gamma_{\mu_2} S(x_3x_4) \gamma_{\mu_1} \psi_a(x_4) D_{\mu_1\mu_4}^\beta(x_1x_4) D_{\mu_2\mu_3}^\beta(x_2x_3). \quad (35)$$

Integration over the time variables in Eq. (35) leads to

$$U_a^{\text{Fig.6}} = -\frac{e^4}{\pi^2} \sum_{n_1 n_2 n_3} \int_{-\infty}^{\infty} \int_{-\infty}^{\infty} d\omega_1 d\omega_2 n_\beta(|\omega_1|) n_\beta(|\omega_2|) \\ \times \left[\frac{1 - \alpha_1 \alpha_4}{r_{14}} \sin(|\omega_1| r_{14}) \right]_{an_1 n_3 a} \left[\frac{1 - \alpha_2 \alpha_3}{r_{23}} \sin(|\omega_2| r_{23}) \right]_{n_2 n_3 n_1 n_2} \\ \times \frac{1}{[E_{n_3}(1-i0) - E_a + \omega_1][E_{n_2}(1-i0) - E_a + \omega_1 + \omega_2][E_{n_1}(1-i0) - E_a + \omega_1]}. \quad (36)$$

Then integration over ω_2 in Eq. (36) can be performed with the use of the Sokhotski-Plemelj theorem:

$$\frac{1}{x \pm i0} = \mathcal{P} \frac{1}{x} \mp \pi i \delta(x), \quad (37)$$

where \mathcal{P} means the principal value of the integral. Taking into account Eq. (37), the imaginary part is

$$\Gamma_a^{\text{Fig.6}} = \frac{2e^4}{\pi} \sum_{n_1 n_2 n_3} \int_{-\infty}^{\infty} \int_{-\infty}^{\infty} d\omega_1 d\omega_2 \frac{n_\beta(|\omega_1|) n_\beta(|\omega_2|) \delta(E_{n_2} - E_a + \omega_1 + \omega_2)}{[E_{n_3}(1-i0) - E_a + \omega_1][E_{n_1}(1-i0) - E_a + \omega_1]} \\ \times \left[\frac{1 - \alpha_1 \alpha_4}{r_{14}} \sin(|\omega_1| r_{14}) \right]_{an_1 n_3 a} \left[\frac{1 - \alpha_2 \alpha_3}{r_{23}} \sin(|\omega_2| r_{23}) \right]_{n_2 n_3 n_1 n_2}$$

$$\begin{aligned}
&= \frac{2e^4}{\pi} \sum_{n_1 n_2 n_3} \left\{ \int_{-\infty}^{\infty} d\omega_1 \int_0^{\infty} d\omega_2 \frac{n_{\beta}(|\omega_1|) n_{\beta}(\omega_2) \delta(E_{n_2} - E_a + \omega_1 - \omega_2)}{[E_{n_3}(1-i0) - E_a + \omega_1][E_{n_1}(1-i0) - E_a + \omega_1]} \right. \\
&\times \left[\frac{1 - \alpha_1 \alpha_4}{r_{14}} \sin(|\omega_1| r_{14}) \right]_{a n_1 n_3 a} \left[\frac{1 - \alpha_2 \alpha_3}{r_{23}} \sin(\omega_2 r_{23}) \right]_{n_2 n_3 n_1 n_2} \\
&+ \int_{-\infty}^{\infty} d\omega_1 \int_0^{\infty} d\omega_2 \frac{n_{\beta}(|\omega_1|) n_{\beta}(\omega_2) \delta(E_{n_2} - E_a + \omega_1 + \omega_2)}{[E_{n_3}(1-i0) - E_a + \omega_1][E_{n_1}(1-i0) - E_a + \omega_1]} \left[\frac{1 - \alpha_1 \alpha_4}{r_{14}} \sin(|\omega_1| r_{14}) \right]_{a n_1 n_3 a} \\
&\times \left. \left[\frac{1 - \alpha_2 \alpha_3}{r_{23}} \sin(\omega_2 r_{23}) \right]_{n_2 n_3 n_1 n_2} \right\}. \tag{38}
\end{aligned}$$

As before, the integration over frequency ω_2 in Eq. (38) differs for $\omega_{n_2 a} < 0$ and $\omega_{n_2 a} > 0$. The result for $\omega_{n_2 a} > 0$ is

$$\begin{aligned}
\Gamma_a^{\text{Fig. 6}} &= \frac{2e^4}{\pi} \sum_{n_1 n_2 n_3} \left\{ \int_0^{|\omega_{n_2 a}|} d\omega \frac{n_{\beta}(\omega) n_{\beta}(|\omega_{n_2 a}| - \omega)}{[E_{n_3}(1-i0) - E_a - \omega][E_{n_1}(1-i0) - E_a - \omega]} \left[\frac{1 - \alpha_1 \alpha_4}{r_{14}} \sin(\omega r_{14}) \right]_{a n_1 n_3 a} \right. \\
&\times \left[\frac{1 - \alpha_2 \alpha_3}{r_{23}} \sin[(|\omega_{n_2 a}| - \omega) r_{23}] \right]_{n_2 n_3 n_1 n_2} \\
&+ \int_{|\omega_{n_2 a}|}^{\infty} d\omega \frac{n_{\beta}(\omega) n_{\beta}(\omega - |\omega_{n_2 a}|)}{[E_{n_3}(1-i0) - E_a - \omega][E_{n_1}(1-i0) - E_a - \omega]} \left[\frac{1 - \alpha_1 \alpha_4}{r_{14}} \sin(\omega r_{14}) \right]_{a n_1 n_3 a} \\
&\times \left[\frac{1 - \alpha_2 \alpha_3}{r_{23}} \sin[(\omega - |\omega_{n_2 a}|) r_{23}] \right]_{n_2 n_3 n_1 n_2} \\
&+ \int_0^{\infty} d\omega \frac{n_{\beta}(\omega) n_{\beta}(|\omega_{n_2 a}| + \omega)}{[E_{n_3}(1-i0) - E_a + \omega][E_{n_1}(1-i0) - E_a + \omega]} \left[\frac{1 - \alpha_1 \alpha_4}{r_{14}} \sin(\omega r_{14}) \right]_{a n_1 n_3 a} \\
&\times \left. \left[\frac{1 - \alpha_2 \alpha_3}{r_{23}} \sin[(|\omega_{n_2 a}| + \omega) r_{23}] \right]_{n_2 n_3 n_1 n_2} \right\}, \tag{39}
\end{aligned}$$

and for $\omega_{n_2 a} < 0$, we have

$$\begin{aligned}
\Gamma_a^{\text{Fig. 6}} &= \frac{2e^4}{\pi} \sum_{n_1 n_2 n_3} \left\{ \int_0^{\infty} d\omega \frac{n_{\beta}(\omega) n_{\beta}(|\omega_{n_2 a}| + \omega)}{[E_{n_3}(1-i0) - E_a - \omega][E_{n_1}(1-i0) - E_a - \omega]} \left[\frac{1 - \alpha_1 \alpha_4}{r_{14}} \sin(\omega r_{14}) \right]_{a n_1 n_3 a} \right. \\
&\times \left[\frac{1 - \alpha_2 \alpha_3}{r_{23}} \sin[(|\omega_{n_2 a}| + \omega) r_{23}] \right]_{n_2 n_3 n_1 n_2} \\
&+ \int_0^{|\omega_{n_2 a}|} d\omega \frac{n_{\beta}(\omega) n_{\beta}(|\omega_{n_2 a}| - \omega)}{[E_{n_3}(1-i0) - E_a + \omega][E_{n_1}(1-i0) - E_a + \omega]} \left[\frac{1 - \alpha_1 \alpha_4}{r_{14}} \sin(\omega r_{14}) \right]_{a n_1 n_3 a} \\
&\times \left[\frac{1 - \alpha_2 \alpha_3}{r_{23}} \sin[(|\omega_{n_2 a}| - \omega) r_{23}] \right]_{n_2 n_3 n_1 n_2} \\
&+ \int_{|\omega_{n_2 a}|}^{\infty} d\omega \frac{n_{\beta}(\omega) n_{\beta}(\omega - |\omega_{n_2 a}|)}{[E_{n_3}(1-i0) - E_a + \omega][E_{n_1}(1-i0) - E_a + \omega]} \left[\frac{1 - \alpha_1 \alpha_4}{r_{14}} \sin(\omega r_{14}) \right]_{a n_1 n_3 a} \\
&\times \left. \left[\frac{1 - \alpha_2 \alpha_3}{r_{23}} \sin[(\omega - |\omega_{n_2 a}|) r_{23}] \right]_{n_2 n_3 n_1 n_2} \right\}. \tag{40}
\end{aligned}$$

E. Thermal loop over thermal loop

The contribution corresponding to the Feynman graph depicted in Fig. 7 is given by the S -matrix element:

$$\hat{S}_{aa}^{(4) \text{ Fig. 7}} = (-ie)^4 \int d^4 x_1 d^4 x_2 d^4 x_3 d^4 x_4 \bar{\psi}_a(x_1) \gamma_{\mu_4} S(x_1 x_2) \gamma_{\mu_3} S(x_2 x_3) \gamma_{\mu_2} S(x_3 x_4) \gamma_{\mu_1} \psi_a(x_4) D_{\mu_1 \mu_4}^{\beta}(x_2 x_4) D_{\mu_2 \mu_3}^{\beta}(x_1 x_3). \tag{41}$$

Integration over the time variables in Eq. (41) yields

$$U_a^{\text{Fig. 7}} = -\frac{e^4}{\pi^2} \sum_{n_1 n_2 n_3} \int_{-\infty}^{\infty} \int_{-\infty}^{\infty} d\omega_1 d\omega_2 n_\beta(|\omega_1|) \left[\frac{1 - \alpha_3 \alpha_1}{r_{31}} \sin(|\omega_1| r_{31}) \right]_{an_2 n_3 n_1} \left[\frac{1 - \alpha_4 \alpha_2}{r_{42}} \sin(|\omega_2| r_{42}) \right]_{n_3 n_1 n_2 a} \\ \times \frac{1}{[E_{n_3}(1-i0) - E_a + \omega_1][E_{n_2}(1-i0) - E_a + \omega_1 + \omega_2][E_{n_1}(1-i0) - E_a + \omega_2]}. \quad (42)$$

Then, substituting Eq. (38) into Eq. (17) and integrating over ω_2 according to the Sokhotski-Plemelj theorem, the result for $\omega_{n_2 a} > 0$ is

$$\Gamma_a^{\text{Fig. 7}} = \frac{2e^4}{\pi} \sum_{n_1 n_2 n_3} \left\{ \int_0^{|\omega_{n_2 a}|} d\omega \frac{n_\beta(\omega) n_\beta(|\omega_{n_2 a}| - \omega)}{[E_{n_3}(1-i0) - E_a - \omega][E_{n_1}(1-i0) - E_{N_2} + \omega]} \left[\frac{1 - \alpha_3 \alpha_1}{r_{31}} \sin(\omega r_{31}) \right]_{an_2 n_3 n_1} \right. \\ \times \left[\frac{1 - \alpha_4 \alpha_2}{r_{42}} \sin[(|\omega_{n_2 a}| - \omega) r_{42}] \right]_{n_3 n_1 n_2 a} \\ + \int_{|\omega_{n_2 a}|}^{\infty} d\omega \frac{n_\beta(\omega) n_\beta(\omega - |\omega_{n_2 a}|)}{[E_{n_3}(1-i0) - E_a - \omega][E_{n_1}(1-i0) - E_{N_2} + \omega]} \left[\frac{1 - \alpha_3 \alpha_1}{r_{31}} \sin(\omega r_{31}) \right]_{an_2 n_3 n_1} \\ \times \left[\frac{1 - \alpha_4 \alpha_2}{r_{42}} \sin[(\omega - |\omega_{n_2 a}|) r_{42}] \right]_{n_3 n_1 n_2 a} \\ + \int_0^{\infty} d\omega \frac{n_\beta(\omega) n_\beta(|\omega_{n_2 a}| + \omega)}{[E_{n_3}(1-i0) - E_a + \omega][E_{n_1}(1-i0) - E_{N_2} - \omega]} \left[\frac{1 - \alpha_3 \alpha_1}{r_{31}} \sin(\omega r_{31}) \right]_{an_2 n_3 n_1} \\ \times \left. \left[\frac{1 - \alpha_4 \alpha_2}{r_{42}} \sin[(|\omega_{n_2 a}| + \omega) r_{42}] \right]_{n_3 n_1 n_2 a} \right\}, \quad (43)$$

and for $\omega_{n_2 a} < 0$, one can obtain

$$\Gamma_a^{\text{Fig. 7}} = \frac{2e^4}{\pi} \sum_{n_1 n_2 n_3} \left\{ \int_0^{\infty} d\omega \frac{n_\beta(\omega) n_\beta(|\omega_{n_2 a}| + \omega)}{[E_{n_3}(1-i0) - E_a - \omega][E_{n_1}(1-i0) - E_{N_2} + \omega]} \left[\frac{1 - \alpha_1 \alpha_4}{r_{14}} \sin(\omega r_{14}) \right]_{an_1 n_3 a} \right. \\ \times \left[\frac{1 - \alpha_2 \alpha_3}{r_{23}} \sin[(|\omega_{n_2 a}| + \omega) r_{23}] \right]_{n_2 n_3 n_1 n_2} \\ + \int_0^{|\omega_{n_2 a}|} d\omega \frac{n_\beta(\omega) n_\beta(|\omega_{n_2 a}| - \omega)}{[E_{n_3}(1-i0) - E_a + \omega][E_{n_1}(1-i0) - E_{N_2} - \omega]} \left[\frac{1 - \alpha_1 \alpha_4}{r_{14}} \sin(\omega r_{14}) \right]_{an_1 n_3 a} \\ \times \left[\frac{1 - \alpha_2 \alpha_3}{r_{23}} \sin[(|\omega_{n_2 a}| - \omega) r_{23}] \right]_{n_2 n_3 n_1 n_2} \\ + \int_{|\omega_{n_2 a}|}^{\infty} d\omega \frac{n_\beta(\omega) n_\beta(\omega - |\omega_{n_2 a}|)}{[E_{n_3}(1-i0) - E_a + \omega][E_{n_1}(1-i0) - E_{N_2} - \omega]} \left[\frac{1 - \alpha_1 \alpha_4}{r_{14}} \sin(\omega r_{14}) \right]_{an_1 n_3 a} \\ \times \left. \left[\frac{1 - \alpha_2 \alpha_3}{r_{23}} \sin[(\omega - |\omega_{n_2 a}|) r_{23}] \right]_{n_2 n_3 n_1 n_2} \right\}. \quad (44)$$

IV. TWO-LOOP DECAY WIDTHS AT FINITE TEMPERATURES: NONRELATIVISTIC LIMIT

In the present section we collect all the contributions above to form the thermal-induced two-photon decay widths. The combination of these contributions should be compared with Eqs. (3) and (5) for the induced two-photon transitions and Raman scattering of thermal photons. This is reasonable to perform in the nonrelativistic limit (see Ref. [56]). Then the matrix elements in Eqs. (25), (26), (29), (30), (33), (34), (39), (40), (43), and (44) can be simplified with

$$\left[\frac{1 - \alpha_i \alpha_j}{r_{ij}} \sin(\omega r_{ij}) \right]_{a(i)b(j)c(i)d(j)} \sim \omega \delta_{ac} \delta_{bd} + \left(-\omega \omega_{ac} \omega_{db} + \frac{\omega^3}{3} \right) \langle a|\mathbf{r}|c\rangle \langle b|\mathbf{r}|d\rangle, \quad (45)$$

where δ_{ab} is the Kronecker symbol and relation $\langle a|\mathbf{p}|b\rangle = i\omega_{ab} \langle a|\mathbf{r}|b\rangle$ is used.

The first term in the right-hand side of Eq. (45) generates infrared divergences of the type $\int_0^\infty d\omega n_\beta(\omega)/\omega$ for each diagram in Figs. 3–7. However, in the sum of loop-inside-loop and loop-over-loop diagrams they arise with different signs and, finally, cancel

each other. This is the ordinary situation occurring for evaluation of the radiative QED corrections to the emission processes [57]. Recently, the same conclusion was verified for the one-loop self-energy corrections at finite temperature [33]. It should be noted here that the regularization of energy shifts suggested in Ref. [34] is also fulfilled in this case. All the divergences arising for each Feynman diagram would be canceled by the coincident limit separately, and the final result would be the same as here. The rigorous proof of this repeats the derivations in previous papers and we omit it for brevity.

To evaluate the terms linear on ω in the sum of all contributions [corresponding to the second term in Eq. (45)], the following equality is helpful [56,58]:

$$\begin{aligned} & \omega(\omega_0 - \omega) \sum_{nn'} \omega_{bn} \omega_{an} \left(\frac{\langle b|\mathbf{r}|n\rangle \langle n|\mathbf{r}|a\rangle}{E_n(1-i0) - E_a + \omega} + \frac{\langle b|\mathbf{r}|n\rangle \langle n|\mathbf{r}|a\rangle}{E_n(1-i0) - E_b - \omega} \right) \omega_{bn'} \omega_{an'} \\ & \times \left(\frac{\langle b|\mathbf{r}|n'\rangle^* \langle n'|\mathbf{r}|a\rangle^*}{E_{n'}(1-i0) - E_a + \omega} + \frac{\langle b|\mathbf{r}|n'\rangle^* \langle n'|\mathbf{r}|a\rangle^*}{E_{n'}(1-i0) - E_b - \omega} \right) \\ & = \omega^3 (\omega_0 - \omega)^3 \sum_{nn'} \left(\frac{\langle b|\mathbf{r}|n\rangle \langle n|\mathbf{r}|a\rangle}{E_n(1-i0) - E_a + \omega} + \frac{\langle b|\mathbf{r}|n\rangle \langle n|\mathbf{r}|a\rangle}{E_n(1-i0) - E_b - \omega} \right) \\ & \times \left(\frac{\langle b|\mathbf{r}|n'\rangle^* \langle n'|\mathbf{r}|a\rangle^*}{E_{n'}(1-i0) - E_a + \omega} + \frac{\langle b|\mathbf{r}|n'\rangle^* \langle n'|\mathbf{r}|a\rangle^*}{E_{n'}(1-i0) - E_b - \omega} \right), \end{aligned} \quad (46)$$

where $\omega_0 = E_a - E_b$.

The combination of Eqs. (25), (26), (29), (30), (33), (34), (39), (40), (43), and (44), as well as the use of Eq. (9) and Eqs. (45), (46), the averaging over projections of the initial state, and the summation over projections of the final state results in the thermal two-photon decay width $\Gamma_a^{2\gamma, \text{BBR}}$. The latter could be presented as a sum of three different contributions: $\Gamma_a^{2\gamma, \text{trans}}$, $\Gamma_a^{2\gamma, \text{ram}}$, and $\Gamma_a^{2\gamma, \text{int}}$. In the absence of resonances, they are associated with two-photon transitions, Raman scattering, and interference between Raman and emission (absorption) branches, respectively. Finally, the total thermal two-photon level width is

$$\Gamma_a^{2\gamma, \text{BBR}} = \sum_b \Gamma_{ab}^{2\gamma, \text{BBR}} = \sum_b (\Gamma_{ab}^{2\gamma, \text{trans}} + \Gamma_{ab}^{2\gamma, \text{ram}} + \Gamma_{ab}^{2\gamma, \text{int}}), \quad (47)$$

where for $b < a$ (i.e., $\omega_{ba} < 0$)

$$\begin{aligned} \Gamma_{ab}^{2\gamma, \text{trans}} &= \frac{4e^4}{9\pi} \frac{1}{2l_a + 1} \lim_{\eta \rightarrow 0} \text{Re} \sum_{m_a m_b} \int_0^{|\omega_{ba}|} d\omega \omega^3 (|\omega_{ba}| - \omega)^3 \sum_{nn'} \left(\frac{\langle b|\mathbf{r}|n\rangle \langle n|\mathbf{r}|a\rangle}{E_n - E_a + \omega + i\eta} + \frac{\langle b|\mathbf{r}|n\rangle \langle n|\mathbf{r}|a\rangle}{E_n - E_b - \omega + i\eta} \right) \\ & \times \left(\frac{\langle b|\mathbf{r}|n'\rangle^* \langle n'|\mathbf{r}|a\rangle^*}{E_{n'} - E_a + \omega + i\eta} + \frac{\langle b|\mathbf{r}|n'\rangle^* \langle n'|\mathbf{r}|a\rangle^*}{E_{n'} - E_b - \omega + i\eta} \right) [n_\beta(\omega) + n_\beta(|\omega_{ba}| - \omega) + n_\beta(\omega)n_\beta(|\omega_{ba}| - \omega)], \end{aligned} \quad (48)$$

$$\begin{aligned} \Gamma_{ab}^{2\gamma, \text{ram}} &= \frac{8e^4}{9\pi} \frac{1}{2l_a + 1} \lim_{\eta \rightarrow 0} \text{Re} \sum_{m_a m_b} \int_0^\infty d\omega \omega^3 (|\omega_{ba}| + \omega)^3 \sum_{nn'} \left(\frac{\langle b|\mathbf{r}|n\rangle \langle n|\mathbf{r}|a\rangle}{E_n - E_a - \omega + i\eta} + \frac{\langle b|\mathbf{r}|n\rangle \langle n|\mathbf{r}|a\rangle}{E_n - E_b + \omega + i\eta} \right) \\ & \times \left(\frac{\langle b|\mathbf{r}|n'\rangle^* \langle n'|\mathbf{r}|a\rangle^*}{E_{n'} - E_a - \omega + i\eta} + \frac{\langle b|\mathbf{r}|n'\rangle^* \langle n'|\mathbf{r}|a\rangle^*}{E_{n'} - E_b + \omega + i\eta} \right) [n_\beta(\omega) + n_\beta(\omega)n_\beta(|\omega_{ba}| + \omega)], \end{aligned} \quad (49)$$

$$\begin{aligned} \Gamma_{ab}^{2\gamma, \text{int}} &= \frac{8e^4}{9\pi} \frac{1}{2l_a + 1} \lim_{\eta \rightarrow 0} \text{Re} \sum_{m_a m_b} \int_{|\omega_{ba}|}^\infty d\omega \omega^3 (\omega - |\omega_{ba}|)^3 \sum_{nn'} \left(\frac{\langle b|\mathbf{r}|n\rangle \langle n|\mathbf{r}|a\rangle}{E_n - E_a + \omega + i\eta} + \frac{\langle b|\mathbf{r}|n\rangle \langle n|\mathbf{r}|a\rangle}{E_n - E_b - \omega + i\eta} \right) \\ & \times \left(\frac{\langle b|\mathbf{r}|n'\rangle^* \langle n'|\mathbf{r}|a\rangle^*}{E_{n'} - E_a + \omega + i\eta} + \frac{\langle b|\mathbf{r}|n'\rangle^* \langle n'|\mathbf{r}|a\rangle^*}{E_{n'} - E_b - \omega + i\eta} \right) n_\beta(\omega)n_\beta(\omega - |\omega_{ba}|), \end{aligned} \quad (50)$$

and for $b > a$ (i.e., $\omega_{ba} > 0$)

$$\begin{aligned} \Gamma_{ab}^{2\gamma, \text{trans}} &= \frac{4e^4}{9\pi} \frac{1}{2l_a + 1} \lim_{\eta \rightarrow 0} \text{Re} \sum_{m_a m_b} \int_0^{|\omega_{ba}|} d\omega \omega^3 (|\omega_{ba}| - \omega)^3 \sum_{nn'} \left(\frac{\langle b|\mathbf{r}|n\rangle \langle n|\mathbf{r}|a\rangle}{E_n - E_a - \omega + i\eta} + \frac{\langle b|\mathbf{r}|n\rangle \langle n|\mathbf{r}|a\rangle}{E_n - E_b + \omega + i\eta} \right) \\ & \times \left(\frac{\langle b|\mathbf{r}|n'\rangle^* \langle n'|\mathbf{r}|a\rangle^*}{E_{n'} - E_a - \omega + i\eta} + \frac{\langle b|\mathbf{r}|n'\rangle^* \langle n'|\mathbf{r}|a\rangle^*}{E_{n'} - E_b + \omega + i\eta} \right) n_\beta(\omega)n_\beta(|\omega_{ba}| - \omega), \end{aligned} \quad (51)$$

$$\begin{aligned} \Gamma_{ab}^{2\gamma, \text{ram}} &= \frac{8e^4}{9\pi} \frac{1}{2l_a + 1} \lim_{\eta \rightarrow 0} \text{Re} \sum_{m_a m_b} \int_{|\omega_{ba}|}^\infty d\omega \omega^3 (\omega - |\omega_{ba}|)^3 \sum_{nn'} \left(\frac{\langle b|\mathbf{r}|n\rangle \langle n|\mathbf{r}|a\rangle}{E_n - E_a - \omega + i\eta} + \frac{\langle b|\mathbf{r}|n\rangle \langle n|\mathbf{r}|a\rangle}{E_n - E_b + \omega + i\eta} \right) \\ & \times \left(\frac{\langle b|\mathbf{r}|n'\rangle^* \langle n'|\mathbf{r}|a\rangle^*}{E_{n'} - E_a - \omega + i\eta} + \frac{\langle b|\mathbf{r}|n'\rangle^* \langle n'|\mathbf{r}|a\rangle^*}{E_{n'} - E_b + \omega + i\eta} \right) [n_\beta(\omega) + n_\beta(\omega)n_\beta(\omega - |\omega_{ba}|)], \end{aligned} \quad (52)$$

TABLE III. Different contributions to the partial two-photon decay width $\Gamma_{2s1s}^{2\gamma, \text{BBR}}$ and the total two-photon decay width Γ_{2s} (in s^{-1}) at different temperatures T (in Kelvin) in H. Values for $\Gamma_{2s1s}^{2\gamma, \text{trans}}$ in the first line coincide with the induced transition rates $W_{2s1s}^{2\gamma, \text{ind}}$ (see Table I), since the cascades are absent for the partial widths. The partial contribution $\Gamma_{2s1s}^{2\gamma, \text{int}}$ is negligibly small at all given temperatures.

T	77	300	1000	3000	5000	10^4
$\Gamma_{2s1s}^{2\gamma, \text{trans}}$	1.358×10^{-4}	2.028×10^{-3}	2.151×10^{-2}	1.731×10^{-1}	4.389×10^{-1}	1.467
$\Gamma_{2s1s}^{2\gamma, \text{ram}}$	1.373×10^{-4}	2.120×10^{-3}	2.500×10^{-2}	2.917×10^{-1}	9.141×10^{-1}	2.455
$\sum_b \Gamma_{2s1s}^{2\gamma, \text{trans}}$	1.358×10^{-4}	2.028×10^{-3}	2.151×10^{-2}	1.732×10^{-1}	4.546×10^{-1}	1.481
$\sum_b \Gamma_{2s1s}^{2\gamma, \text{ram}}$	1.373×10^{-4}	2.120×10^{-3}	2.500×10^{-2}	2.916×10^{-1}	9.039×10^{-1}	2.395
$\sum_b \Gamma_{2s1s}^{2\gamma, \text{int}}$	1.677×10^{-17}	3.466×10^{-13}	1.655×10^{-9}	2.452×10^{-5}	1.511×10^{-3}	5.972×10^{-2}
$\sum_b \Gamma_{2s1s}^{2\gamma, \text{trans+ram+int}}$	2.731×10^{-4}	4.148×10^{-3}	4.651×10^{-2}	4.648×10^{-1}	13.600×10^{-1}	3.936

$$\Gamma_{ab}^{2\gamma, \text{int}} = \frac{8e^4}{9\pi} \frac{1}{2l_a + 1} \lim_{\eta \rightarrow 0} \text{Re} \sum_{m_a m_b} \int_0^\infty d\omega \omega^3 (|\omega_{ba}| + \omega)^3 \sum_{n n'} \left(\frac{\langle b|\mathbf{r}|n\rangle \langle n|\mathbf{r}|a\rangle}{E_n - E_a + \omega + i\eta} + \frac{\langle b|\mathbf{r}|n\rangle \langle n|\mathbf{r}|a\rangle}{E_n - E_b - \omega + i\eta} \right) \times \left(\frac{\langle b|\mathbf{r}|n'\rangle^* \langle n'|\mathbf{r}|a\rangle^*}{E_{n'} - E_a + \omega + i\eta} + \frac{\langle b|\mathbf{r}|n'\rangle^* \langle n'|\mathbf{r}|a\rangle^*}{E_{n'} - E_b - \omega + i\eta} \right) n_\beta(\omega) n_\beta(|\omega_{ba}| + \omega). \quad (53)$$

From the expressions above, it follows that their structure is similar to the ordinary “zero-temperature” two-photon decay widths (see Ref. [23]). In the absence of the resonant intermediate states in the sum over n , Eqs. (48) and (51), the imaginary infinitesimal part $i\eta$ in each energy denominator can be omitted. The situation is slightly different for the Raman-like contributions given by Eqs. (49) and (52). Since the integration interval over the frequency ω in these equations is presented by the real half-axis, there are an infinite number of resonances for any initial and final states a and b . Therefore, the contributions (49) and (52) cannot be interpreted as the pure Raman scattering rate expressed by Eq. (5). The same holds for the remaining interference contributions, Eqs. (50) and (53). Their algebraic structure allows one to validate that this is the interference contribution between Raman and emission (absorption) branches.

We can conclude that the contributions Eqs. (48) and (51) are equal to transition rates given by Eqs. (3) and (4), respectively, only in the absence of resonant intermediate states. However, for the total width equation, Eq. (47), where summation over all possible final states b is performed, such states are always existing and calculation of $\Gamma_a^{2\gamma, \text{BBR}}$ should be performed with the use of Eq. (9). In contrast to this, the two-photon transition rate equations, Eqs. (3) and (4), require the regularization by introducing the level widths into the denominators [23]. It is important to note that within the two-loop approach summation over final states b arises immediately in a full analogy with the well-known QED derivation of one-photon level widths via the imaginary part of the one-loop self-energy (see, for example, Ref. [56]).

Numerical calculations with the summation over the entire spectrum in Eqs. (2)–(5) for the transition rates and the thermal two-photon decay widths in Eqs. (48)–(53) were performed with the use of the B-spline method [59]. The results for $2s$ and $3s$ states in H and He^+ atoms are presented in Tables I–VI.

V. DISCUSSION AND CONCLUSIONS

In this paper, we have considered thermal two-loop self-energy corrections. Their imaginary part represents the two-photon thermal correction to the natural (spontaneous) width of the atomic energy level. In general, the total contribution can be expressed by Eqs. (47)–(53). Then, according to

Eqs. (13) and (14), the contribution Γ_a^{BBR} should be compared with others “ordinary” radiative QED corrections and with the BBR-induced rates known from the quantum mechanical approach.

The relativistic and “zero-temperature” QED corrections (see Ref. [60]) of the leading order to the $2s$ level width in the

TABLE IV. Different contributions to the partial two-photon decay width $\Gamma_{3s1s}^{2\gamma, \text{BBR}}$ and the total two-photon decay width Γ_{3s} (in s^{-1}) at different temperatures T (in Kelvin) in H. The partial contribution $\Gamma_{3s1s}^{2\gamma, \text{int}}$ is negligibly small at all given temperatures. The zero-temperature two-photon width is $\Gamma_{3s1s}^{2\gamma} = 2.082854 \text{ s}^{-1}$.

T	77	300	1000	3000	5000	10^4
$\Gamma_{3s1s}^{2\gamma, \text{trans}}$	2.161×10^{-4}	3.179×10^{-3}	3.268×10^{-2}	2.632×10^{-1}	6.707×10^{-1}	1.924
$\Gamma_{3s1s}^{2\gamma, \text{ram}}$	2.214×10^{-4}	3.498×10^{-3}	4.751×10^{-2}	3.980×10^{-1}	6.675×10^{-1}	6.822×10^{-1}
$\sum_b \Gamma_{3s1s}^{2\gamma, \text{trans}}$	2.382×10^{-4}	3.500×10^{-3}	3.585×10^{-2}	2.863×10^{-1}	7.253×10^{-1}	2.116
$\sum_b \Gamma_{3s1s}^{2\gamma, \text{ram}}$	2.442×10^{-4}	3.863×10^{-3}	5.275×10^{-2}	4.390×10^{-1}	7.386×10^{-1}	9.513×10^{-1}
$\sum_b \Gamma_{3s1s}^{2\gamma, \text{int}}$	1.285×10^{-15}	2.731×10^{-11}	5.862×10^{-7}	8.614×10^{-4}	7.269×10^{-3}	8.337×10^{-2}
$\sum_b \Gamma_{3s1s}^{2\gamma, \text{trans+ram+int}}$	4.824×10^{-4}	7.363×10^{-3}	8.860×10^{-2}	7.261×10^{-1}	1.471	3.151

TABLE V. Different contributions to the partial two-photon decay width $\Gamma_{2s1s}^{2\gamma,\text{BBR}}$ and the total thermal two-photon decay width Γ_{2s} (in s^{-1}) at different temperatures T (in Kelvin) in He^+ . The partial contribution $\Gamma_{2s1s}^{2\gamma,\text{int}}$ is negligibly small at all given temperatures.

T	77	300	1000	3000	5000	10^4
$\Gamma_{2s1s}^{2\gamma,\text{trans}}$	5.438×10^{-4}	8.243×10^{-3}	9.044×10^{-2}	7.868×10^{-1}	2.118	7.893
$\Gamma_{2s1s}^{2\gamma,\text{ram}}$	5.468×10^{-4}	8.335×10^{-3}	9.385×10^{-2}	8.801×10^{-1}	2.562	12.072
$\sum_b \Gamma_{2sb}^{2\gamma,\text{trans}}$	5.452×10^{-4}	8.243×10^{-3}	9.044×10^{-2}	7.868×10^{-1}	2.118	7.894
$\sum_b \Gamma_{2sb}^{2\gamma,\text{ram}}$	5.468×10^{-4}	8.335×10^{-3}	9.385×10^{-2}	8.801×10^{-1}	2.562	12.08
$\sum_b \Gamma_{2sb}^{2\gamma,\text{int}}$	6.546×10^{-20}	1.351×10^{-15}	6.183×10^{-12}	1.384×10^{-8}	5.241×10^{-7}	2.558×10^{-4}
$\sum_b \Gamma_{2s}^{2\gamma,\text{trans+ram+int}}$	10.880×10^{-4}	1.658×10^{-2}	1.843×10^{-1}	1.667	2.774	19.974

nonrecoil limit are given by

$$\tilde{W}_{ab}^{2\gamma,\text{spon}} = W_{ab}^{2\gamma,\text{spon}}[1 + \epsilon^{\text{rel}} + \epsilon^{\text{QED}}], \quad (54)$$

where

$$\epsilon^{\text{rel}} = c_2(\alpha Z)^2, \quad (55)$$

$$\epsilon^{\text{QED}} = c_3 \frac{\alpha}{\pi} (\alpha Z)^2 \ln[(\alpha Z)^{-2}]. \quad (56)$$

The coefficients c_2 and c_3 in the equation above were evaluated for the two-photon decay rate of higher excited ns and nd states in Ref. [60]. Using numerical values of the parameters c_2 and c_3 , one can find that the relativistic and radiative QED corrections to the $2s \rightarrow 1s + \gamma(E1)$ transition in H atoms are equal to -2.908×10^{-4} and $-2.024 \times 10^{-5} \text{ s}^{-1}$, respectively. The depopulation rates with the account for the finite lifetimes and the thermal two-photon level widths of the $2s$ state at room temperature are $\Gamma_{2s}^{1\gamma,\text{BBR-QED}} = 4.159 \times 10^{-3} \text{ s}^{-1}$ and $\sum_b \Gamma_{2sb}^{2\gamma,\text{trans+ram+int}} = 4.148 \times 10^{-3} \text{ s}^{-1}$ (see Tables II and III). Thus, the two-loop thermal corrections to the $2s$ level broadening in H atoms dominate over the relativistic and radiative corrections. However, all these corrections are still less than the experimental uncertainty in measuring the lifetime of the $2s$ state in hydrogen (see Table VII).

The situation is different for the $2s$ state in the He^+ atom, where more accurate experiments were carried out, and the measured decay rate is $525 \pm 5 \text{ s}^{-1}$ [43]. According to Eq. (54) the relativistic and radiative QED corrections to the $2s$ - $1s$ transition in He^+ atoms are -7.445×10^{-2} and $-4.451 \times 10^{-3} \text{ s}^{-1}$, respectively. Assuming that the experiment [43] is carried out at room temperature, one can find the corresponding BBR-induced depopulation rate $\Gamma_{2s}^{1\gamma,\text{BBR-QED}} = 1.720 \times 10^{-2} \text{ s}^{-1}$ and the total thermal two-photon width $\sum_b \Gamma_{2sb}^{2\gamma,\text{trans+ram+int}} = 1.658 \times 10^{-2} \text{ s}^{-1}$ (see

Table V). Again, the two-loop thermal corrections to the $2s$ level broadening at $T = 300 \text{ K}$ in the He^+ ion reach the same order as the one-photon depopulation width at higher temperatures. Although the contribution of thermal corrections is 2 orders less than the experimental uncertainty, the further improvement of accuracy could verify directly this effect. The current status of experiments on the measurement of the $2s$ state lifetime in other H-like ions is presented in Table VII.

Except for the He^+ results, the precision on the level of 1% is also achieved for Ar^{17+} and Ni^{27+} hydrogenlike ions. However, since the Planck distribution function is mainly in the low-frequency region at low temperatures one can neglect ω in the energy denominators of Eqs. (48)–(53). This leads to the parametric estimation $(k_B T)^4 / (m^3 Z^2)$ r.u. (relativistic units) for the $\Gamma_{2s}^{2\gamma,\text{BBR}}$ contribution in the low-temperature regime. Keeping in mind that $k_B T \sim m(\alpha Z)^2$ in r.u., the well-known αZ parametrization can be found in the form $m\alpha^2(\alpha Z)^6$ for the two-photon contribution $\Gamma_{2s}^{2\gamma,\text{BBR}}$. It follows that $\Gamma_{2s}^{2\gamma,\text{BBR}}$ behaves like Z^6 ; however, at high values of Z and room temperature, the total contribution is damped by the distant Planck tails, where the characteristic transition energies are concentrated for a given Z . Using this estimation, numerical calculations show that the thermal effect described in this paper is much less than the uncertainty of the experiments listed in Table VII. The calculations performed in the present work could be easily extended to the case of many-electron atoms where two-photon decays of K -shell vacancies are also the subject of theoretical and experimental investigations [61–64].

It is also interesting to note the peculiarity of the total Raman-like contribution $\sum_b \Gamma_{ab}^{2\gamma,\text{ram}}$ to the two-photon level broadening. As seen from Table III the total value $\sum_b \Gamma_{ab}^{2\gamma,\text{ram}}$ at some temperatures becomes less than the partial contribu-

TABLE VI. Different contributions to the partial two-photon decay width $\Gamma_{3s1s}^{2\gamma,\text{BBR}}$ and the total thermal two-photon decay width Γ_{3s} (in s^{-1}) at different temperatures T (in Kelvin) in He^+ . The partial contribution $\Gamma_{3s1s}^{2\gamma,\text{int}}$ is negligibly small at all given temperatures. The zero-temperature two-photon widths is $\Gamma_{3s1s}^{2\gamma} = 1.333 \times 10^2 \text{ s}^{-1}$.

T	77	300	1000	3000	5000	10^4
$\Gamma_{3s1s}^{2\gamma,\text{trans}}$	8.722×10^{-4}	1.312×10^{-2}	1.422×10^{-1}	1.206	3.197	11.90
$\Gamma_{3s1s}^{2\gamma,\text{ram}}$	8.772×10^{-4}	1.344×10^{-2}	1.540×10^{-1}	1.571	5.088	19.610
$\sum_b \Gamma_{3sb}^{2\gamma,\text{trans}}$	9.615×10^{-4}	1.447×10^{-2}	1.566×10^{-1}	1.325	3.504	12.97
$\sum_b \Gamma_{3sb}^{2\gamma,\text{ram}}$	9.674×10^{-4}	1.482×10^{-2}	1.700×10^{-1}	1.741	5.652	21.670
$\sum_b \Gamma_{3sb}^{2\gamma,\text{int}}$	4.997×10^{-18}	1.031×10^{-13}	4.823×10^{-10}	2.267×10^{-6}	2.727×10^{-4}	2.313×10^{-2}
$\sum_b \Gamma_{3s}^{2\gamma,\text{trans+ram+int}}$	1.929×10^{-3}	2.929×10^{-2}	3.266×10^{-1}	3.066	9.156	34.663

TABLE VII. Comparison of the experimental and theoretical lifetimes $\tau_{2s} = \Gamma_{2s}^{-1}$ (in s) of the $2s$ level in H-like ions. Theoretical values of τ_{2s} and $\Gamma_{2s}^{2\gamma}$ were calculated in a fully relativistic approach with the account for finite nuclear size effects. The relativistic calculation of the $M1$ decay rate $2s \rightarrow 1s + \gamma(M1)$ is also taken into account. In the last column values for $\Gamma_{2s}^{2\gamma, \text{BBR}}$ at $T = 300$ K are estimated within the nonrelativistic approach.

Z	Experiment τ_{2s} (s)	Theory τ_{2s} (s)	Theory $\Gamma_{2s}^{2\gamma}$ (s^{-1})	Theory $\Gamma_{2s}^{2\gamma, \text{BBR}}$ (s^{-1})
1	0.67 ± 0.29^a $0.12_{-0.04}^{+0.03b}$	1.215×10^{-1}	8.229	4.148×10^{-3}
2	$(1.922 \pm 0.082) \times 10^{-3}^c$ $(2.04_{-0.34}^{+0.81}) \times 10^{-3}^d$ $(1.905 \pm 0.018) \times 10^{-3e}$	1.899×10^{-3}	526.607	1.658×10^{-2}
8	$(4.53 \pm 0.43) \times 10^{-7f}$	4.640×10^{-7}	2.155×10^6	2.652×10^{-1}
9	$(2.37 \pm 0.19) \times 10^{-7f}$	2.288×10^{-7}	4.370×10^6	3.357×10^{-1}
16	$(7.3 \pm 0.7) \times 10^{-9g}$	7.161×10^{-9}	1.396×10^8	1.061
18	$(3.54 \pm 0.25) \times 10^{-9g}$ $(3.487 \pm 0.036) \times 10^{-9h}$	3.498×10^{-9}	2.859×10^8	1.343
28	$(2.171 \pm 0.018) \times 10^{-10i}$	2.157×10^{-10}	4.636×10^9	1.625
36	$(3.68 \pm 0.14) \times 10^{-11j}$	3.703×10^{-11}	2.700×10^{10}	2.685

^aReference [38]; ^bReference [35] (this value is extracted from the analysis of CMB); ^cReference [40]; ^dReference [65]; ^eReference [43]; ^fReference [41]; ^gReference [42]; ^hReference [44]; ⁱReference [46]; ^jReference [45].

tion $\Gamma_{ab}^{2\gamma, \text{ram}}$. This occurs via the contributions with $b > a$ in the sum over b in Eq. (52). They change the sign with the increasing of temperature and, as a result, this leads to the decreasing of the total value. The same situation is well known for the thermal Stark shift (see, for example, Refs. [28,47]). Such behavior of partial contributions, namely, that they can be negative, was found previously in Ref. [23]. In addition, the numerical calculations showed that all two-photon contributions proportional to $n_\beta(\omega)n_\beta(\omega')$ are negligible at reasonable temperatures. In particular, it was found that the interference part given by Eqs. (50) and (53), as well as the absorptionlike part given by Eq. (51), does not make a tangible contribution to the thermal two-photon width.

The corrections found in this work can also play an important role in describing the cosmological recombination processes. The standard calculation of the ionization fraction of the primordial hydrogen plasma takes into account only the induced two-photon decay and Raman scattering.

In Refs. [25–27] it was shown that the induced two-photon transition $2s \rightarrow 1s + 2\gamma$ corrects the ionization fraction on the level of a few percent. The two-loop thermal corrections for the $2s$ level width listed in Table III are several times larger than the corresponding induced rates at recombination temperatures ($1000 < T < 5000$). Thus, one can expect the contribution to the ionization fraction at the same level.

In conclusion, we can expect that the radiative temperature-dependent corrections to the level widths found in this paper will play a role in both astrophysical and laboratory investigations. At least, a further increase of the experimental accuracy requires the need to take these corrections into account.

ACKNOWLEDGMENT

This work was supported by the Russian Science Foundation (Grant No. 17-12-01035).

- | | |
|--|--|
| <p>[1] J. A. Rubiño-Martin and R. A. Sunyaev, <i>Astron. Lett.</i> 44, 1 (2018).</p> <p>[2] T. Zalialiutdinov, D. Solovyeu, L. Labzowsky, and G. Plunien, <i>Phys. Rev. A</i> 91, 033417 (2015).</p> <p>[3] W. J. Marciano, C. Zhang, and S. Willenbrock, <i>Phys. Rev. D</i> 85, 013002 (2012).</p> <p>[4] D. English, V. V. Yashchuk, and D. Budker, <i>Phys. Rev. Lett.</i> 104, 253604 (2010).</p> <p>[5] P. Cancio Pastor, I. Galli, G. Giusfredi, D. Mazzotti, and P. De Natale, <i>Phys. Rev. A</i> 92, 063820 (2015).</p> <p>[6] X. Feng, S. Aoki, H. Fukaya, S. Hashimoto, Ta. Kaneko, J. I. Noaki, and E. Shintani, <i>Phys. Rev. Lett.</i> 109, 182001 (2012).</p> <p>[7] K. W. Martin, G. Phelps, N. D. Lemke, M. S. Bigelow, B. Stuhl, M. Wojcik, M. Holt, I. Coddington, M. W. Bishop, and J. H. Burke, <i>Phys. Rev. Appl.</i> 9, 014019 (2018).</p> | <p>[8] J. Chluba and R. Sunyaev, <i>Astron. Astrophys.</i> 480, 629 (2008).</p> <p>[9] M. Göppert Mayer, <i>Ann. Phys. (Leipzig, Germany)</i> 401, 273 (1931).</p> <p>[10] Planck Collaboration, Planck 2015 results. XIII. Cosmological parameters, <i>Astron. Astrophys.</i> 594, A13 (2016).</p> <p>[11] Ya. Zel'dovich, V. Kurt, and R. Sunyaev, <i>Zh. Exsp. Teor. Fiz.</i> 55, 278 (1968) [<i>Sov. Phys. JETP Lett.</i> 28, 146 (1969)].</p> <p>[12] P. J. E. Peebles, <i>Astrophys. J.</i> 153, 1 (1968).</p> <p>[13] C. M. Hirata, <i>Phys. Rev. D</i> 78, 023001 (2008).</p> <p>[14] D. Solovyeu, V. Dubrovich, A. Volotka, L. Labzowsky, and G. Plunien, <i>J. Phys. B</i> 43, 175001 (2010).</p> <p>[15] L. N. Labzowsky and A. V. Shonin, <i>Phys. Rev. A</i> 69, 012503 (2004).</p> <p>[16] L. Labzowsky, D. Solovyeu, and G. Plunien, <i>Phys. Rev. A</i> 80, 062514 (2009).</p> |
|--|--|

- [17] T. A. Zalyalyutdinov, D. A. Solovyev, and L. N. Labzovskii, *Opt. Spectrosc.* **110**, 328 (2011).
- [18] U. Jentschura, *J. Phys. A* **40**, F223 (2007).
- [19] U. Jentschura, *J. Phys. A* **41**, 155307 (2008).
- [20] U. D. Jentschura, *Phys. Rev. A* **79**, 022510 (2009).
- [21] U. D. Jentschura and A. Surzhykov, *Phys. Rev. A* **77**, 042507 (2008).
- [22] O. Yu. Andreev, L. Labzowsky, G. Plunien, and D. Solovyev, *Phys. Rep.* **455**, 135 (2008).
- [23] T. Zalialiutdinov, D. Solovyev, L. Labzowsky, and G. Plunien, *Phys. Rev. A* **89**, 052502 (2014).
- [24] T. A. Zalialiutdinov, D. A. Solovyev, L. N. Labzowsky, and G. Plunien, *Phys. Rep.* **737**, 1 (2018).
- [25] J. Chluba and R. Sunyaev, *Astron. Astrophys.* **446**, 39 (2006).
- [26] C. M. Hirata and E. R. Switzer, *Phys. Rev. D* **77**, 083007 (2008).
- [27] E. Kholupenko and A. Ivanhik, *Astron. Lett.* **32**, 795 (2006).
- [28] D. Solovyev, L. Labzowsky, and G. Plunien, *Phys. Rev. A* **92**, 022508 (2015).
- [29] T. Zalialiutdinov, D. Solovyev, L. Labzowsky, and G. Plunien, *Phys. Rev. A* **96**, 012512 (2017).
- [30] T. Zalialiutdinov, D. Solovyev, and L. Labzowsky, *J. Phys. B* **51**, 015003 (2018).
- [31] T. Zalialiutdinov, D. Solovyev, L. Labzowsky, and G. Plunien, *Phys. Rev. A* **99**, 012502 (2019).
- [32] D. Solovyev, T. Zalialiutdinov, A. Anikin, J. Triaskin, and L. Labzowsky, *Phys. Rev. A* **100**, 012506 (2019).
- [33] T. Zalialiutdinov, D. Solovyev, and L. Labzowsky, *Phys. Rev. A* **101**, 052503 (2020).
- [34] D. Solovyev, *Ann. Phys.* **415**, 168128 (2020).
- [35] V. Mukhanov, J. Kim, P. Naselsky, T. Trombetti, and C. Burigana, *J. Cosmol. Astropart. Phys.* (2012) 040.
- [36] C. L. Cesar, D. G. Fried, T. C. Killian, A. D. Polcyn, J. C. Sandberg, I. A. Yu, T. J. Greytak, D. Kleppner, and J. M. Doyle, *Phys. Rev. Lett.* **77**, 255 (1996).
- [37] D. O'Connell, K. J. Kollath, A. J. Duncan, and H. Kleinpoppen, *J. Phys. B* **8**, L214 (1975).
- [38] H. Krüger and A. Oed, *Phys. Lett. A* **54**, 251 (1975).
- [39] M. Lipeles, R. Novick, and N. Tolk, *Phys. Rev. Lett.* **15**, 690 (1965).
- [40] M. H. Prior, *Phys. Rev. Lett.* **29**, 611 (1972).
- [41] C. L. Cocke, B. Curnutte, J. R. Macdonald, J. A. Bedner, and R. Marrus, *Phys. Rev. A* **9**, 2242 (1974).
- [42] R. Marrus and R. W. Schmieder, *Phys. Rev. A* **5**, 1160 (1970).
- [43] E. A. Hinds, J. E. Clendenin, and R. Novick, *Phys. Rev. A* **17**, 670 (1978).
- [44] H. Gould and R. Marrus, *Phys. Rev. A* **28**, 2001 (1983).
- [45] S. Cheng, H. G. Berry, R. W. Dunford, D. S. Gemmell, E. P. Kanter, B. J. Zabransky, A. E. Livingston, L. J. Curtis, J. Bailey, and J. A. Nolen, Jr., *Phys. Rev. A* **47**, 903 (1993).
- [46] R. W. Dunford, M. Hass, E. Bakke, H. G. Berry, C. J. Liu, and M. L. A. Raphaelian, and L. J. Curtis, *Phys. Rev. Lett.* **62**, 2809 (1989).
- [47] J. W. Farley and W. H. Wing, *Phys. Rev. A* **23**, 2397 (1981).
- [48] T. F. Gallagher and W. E. Cooke, *Phys. Rev. Lett.* **42**, 835 (1979).
- [49] S. P. Goldman and G. W. F. Drake, *Phys. Rev. A* **24**, 183 (1981).
- [50] A. I. Akhiezer and V. B. Berestetskii, *Quantum Electrodynamics*, Interscience Monographs and Texts in Physics and Astronomy (Interscience, New York, 1965).
- [51] T. Zalialiutdinov, Yu. Baukina, D. Solovyev, and L. Labzowsky, *J. Phys. B* **47**, 115007 (2014).
- [52] N. Bezginov, T. Valdez, M. Horbatsch, A. Marsman, A. C. Vutha, and E. A. Hessels, *Science* **365**, 1007 (2019).
- [53] U. D. Jentschura and M. Haas, *Phys. Rev. A* **78**, 042504 (2008).
- [54] J. Sapirstein, K. Pachucki, and K. T. Cheng, *Phys. Rev. A* **69**, 022113 (2004).
- [55] J. Sucher, *Phys. Rev.* **107**, 1448 (1957).
- [56] L. Labzowsky, G. Klimchitskaya, and Y. Y. Dmitriev, *Relativistic Effects in the Spectra of Atomic Systems* (CRC, Boca Raton, FL, 1993).
- [57] V. M. Shabaev, *Phys. Rep.* **356**, 3, 119 (2002).
- [58] U. D. Jentschura and C. M. Adhikari, *Phys. Rev. A* **97**, 062120 (2018).
- [59] V. M. Shabaev, I. I. Tupitsyn, V. A. Yerokhin, G. Plunien, and G. Soff, *Phys. Rev. Lett.* **93**, 130405 (2004).
- [60] B. J. Wundt and U. D. Jentschura, *Phys. Rev. A* **80**, 022505 (2009).
- [61] K. Ilakovaca, M. Uroic, M. Majer, S. Pasic, and B. Vukovic, *Radiat. Phys. Chem.* **75**, 1451 (2006).
- [62] P. H. Mokler and R. W. Dunford, *Phys. Scr.* **69**, C1 (2004).
- [63] T. Jahrsetz, Two-photon processes in highly charged ions, Ph.D. thesis, Universität Heidelberg, 2015.
- [64] F. A. Parpia and W. R. Johnson, *Phys. Rev. A* **26**, 1142(R) (1982).
- [65] C. A. Kocher, J. E. Clendenin, and R. Novick, *Phys. Rev. Lett.* **29**, 615 (1972).